Effect of unplanned block in volleyball on joint coordination during landing

Auteur : Dantinne, Charline
Promoteur(s) : Schwartz, Cédric
Faculté : Faculté des Sciences appliquées
Diplôme : Master en ingénieur civil biomédical, à finalité spécialisée
Année académique : 2024-2025
URI/URL : http://hdl.handle.net/2268.2/23319

University of Liège - Faculty of Applied Sciences

MASTER'S THESIS

Effect of unplanned block in volleyball on joint coordination during landing

Master's thesis completed to obtain the degree of Master of Science in Biomedical Engineering by

Dantinne Charline

Supervisor:

Prof. Cédric Schwartz

Academic year 2024-2025

Acknowledgement

Before beginning this thesis, I wish to thank everyone who, directly or indirectly, supported me.

First, I want to express my sincere gratitude to my supervisor, Professor Cédric Schwartz, whose guidance made this thesis possible. He proposed a research topic perfectly suited to my interests and generously devoted his time and expertise throughout the project. I am especially grateful for the access he granted me to the Human Movement Analysis Laboratory and for the trust he placed in me to handle all the necessary equipment.

I would like to thank my friends who volunteered as participants to this work. The data they helped generate form the very foundation of this study. Their enthusiasm and perseverance, especially when sessions did not go as planned, and the time they generously devoted made the completion of this work possible.

I would also like to thank Corinne Léonard, a physiotherapy student, with whom I carried out the testing phase. It was a real pleasure to collaborate with her, as we were able to share not only our mutual interest and experience in volleyball, but also our complementary academic perspectives, hers in physiotherapy and mine in engineering.

I am truly grateful to my family and friends for their unwavering support, encouragement, and advice during my studies. Their help over the past five years has been invaluable.

Finally, I acknowledge all those not explicitly mentioned who nonetheless contributed to the completion of this work.

Abstract

Understanding joint coordination during landing is essential in volleyball, a sport requiring explosive movements and rapid transitions. This study investigates inter-joint coordination in the landing phase following a block, focusing on the effects of planned versus unplanned conditions and gender-related differences. Twenty volleyball players (10 male, 10 female), competing at national to professional level in Belgium, participated in a laboratory-based protocol involving three-step block jumps under both planned (known direction) and unplanned (direction revealed at movement onset) conditions. Kinematic data, ground reaction forces (GRF), and surface electromyography were recorded using a motion capture system, force plates, and wireless sensors.

Joint coordination was assessed using classical biomechanical analysis, Principal Component Analysis (PCA), and Statistical Parametric Mapping (SPM1D). Minimal differences were observed between planned and unplanned landings, suggesting a shared global motor strategy. This may be due to the timing of direction cues and task constraints, such as the requirement to land on force plates.

Sex differences were more pronounced. Female athletes showed more consistent, distal-joint-dominated patterns, while males relied more on proximal joints and demonstrated greater variability. GRF analysis supported these trends, with females exhibiting smoother force profiles. A consistent asymmetry between lead and trail legs was observed, likely reflecting task-specific movement organization.

These results emphasize the need to consider sex-specific strategies in training and highlight the usefulness of multivariate methods like PCA in uncovering coordination patterns.

Table of Contents

List of Figures

Introduction

Volleyball is one of the most widely played sports globally, with more than 220 national federations registered under the *Fédération Internationale de Volleyball* (FIVB). This sport requires speed, reaction speed, coordination and strength to be able to play at higher levels. In general, each player has a specific role, with distinct physical and technical demands. The setter acts as the playmaker, distributing the ball to the hitters, whose aim is scoring a point. Hitters are generally tall and explosive, allowing them to reach higher contact points. The libero, by contrast, is a defensive specialist, focused on receiving serves and attacks from the opposing team. Among the key actions in volleyball are the reception of a serve or a spike, the setting, the attack and the block. The latter is a defensive move aimed at stopping the opponent's attack at the net. This action is of particular interest in this study, especially regarding hitters who transition rapidly between block and attack roles. To perform an effective block, players typically use a specific footwork pattern, often a two- or three-step sequence, depending on their starting position and the side of the court where the block is required. For example, from the center of the court, if the ball is set to the right, the player typically performs a right-left-right step sequence before jumping, and vice versa for the left side. In a two-step sequence, the initial step is omitted.

These repeated actions expose players to frequent jump-landing tasks, especially during block attempts and after receptions. Consequently, volleyball players are subjected to significant biomechanical stress, particularly on the lower limbs. According to sports injury statistics, lower extremity injuries account for more than 50% of all volleyball injuries [1]. Ankles and knees are the most commonly affected areas, with injuries such as sprains, ligament tears, or fractures.

In this context, a deeper understanding of biomechanics during this specific action of blocking, is essential. It can help identify risk factors, improve injury prevention strategies, and ultimately enhance player performance and safety. This study focuses on the intersection

between performance optimization, specifically jump mechanics during blocking, and injury risk, with particular attention to lower limb joint coordination. Given the biomechanical demands of blocking actions in volleyball and the potential for injury, it is crucial to understand how coordination patterns differ between planned and unplanned actions. This study aims to explore whether there are significant differences in the joint coordination of the lower limbs when players perform planned versus unplanned blocking movements.

To achieve this objective, this work begins with an in-depth review of the literature in Chapter 1. It first considers how sport-specific movements are associated with injury risks. The review then explores how anticipation and task predictability can influence motor control and performance. Particular attention is given to how joint coordination is defined and to the methods commonly used to assess inter-joint coordination.

Chapter 2 then provides a detailed description of the experimental protocol conducted in a controlled laboratory environment to ensure accurate data collection from twenty participants. It outlines the tasks performed by the volunteers, as well as the equipment and infrastructure used. This chapter also explains, in detail, the various data processing steps applied to extract the relevant information required for analyzing inter-joint coordination.

Chapter 3 presents and analyzes the results of this study using two key methods : principal component analysis (PCA) to assess joint coordination patterns, and one-dimensional statistical parametric mapping (SPM1D) as a statistical tool for quantitative results. The primary objective of this chapter is to identify coordination patterns and examine differences between conditions. Specifically, comparisons are made between planned and unplanned trials, as well as between male and female participants. Additional discussion is provided to interpret and better understand the observed differences.

The limitations of this study are outlined in Chapter 4, providing a clear perspective on the challenges encountered and highlighting opportunities for future research.

The thesis concludes by highlighting the main insights gained and their implications for sports performance and injury prevention, while also identifying directions for future research.

Chapter 1

State of the art

This chapter provides a comprehensive overview of the theoretical and experimental background necessary to understand the mechanisms of joint coordination in dynamic sports movements. The focus is placed on how planned and unplanned scenarios influence inter-joint coordination, particularly in tasks such as landing and sidestepping, which are known to be associated with a high risk of lower limb injuries. The chapter first explores the biomechanical demands of sport-specific actions and their connection to injury risks. It then introduces the concept of anticipation and its impact on motor control and joint mechanics. The notion of joint coordination is further developed, emphasizing its relevance in understanding movement adaptations under different constraints. Finally, the chapter presents the main approaches used to quantify inter-joint coordination based on kinematic data, highlighting their strengths and limitations in capturing the complexity of human movement.

1.1 Sport-specific movements and Injury risks

Understanding movement patterns in sports is crucial in identifying the mechanisms and risk factors associated with lower limb injuries. Rapid changes in acceleration, such as those occurring during landings and directional changes, challenge the neuromuscular system and are commonly linked to injuries such as anterior cruciate ligament (ACL) ruptures or ankle sprains. These movements require athletes to react to external stimuli, often leading to modifications in joint mechanics and increased stress on the knee, especially in unanticipated sidestepping and landing scenarios [2, 3, 4].

Fatigue is another critical factor influencing limb kinematics and kinetics, as it affects movement efficiency, stabilization and especially coordination. These impairments can increase the risk of injury by disrupting proper joint mechanics during intense activities. The plasticity of the motor control system allows adaptation to external and internal changes, such as fatigue. In this context, studying inter-joint coordination becomes particularly relevant as it reflects how the musculoskeletal system adapts its control strategies to maintain performance under such conditions.

Variability in movement coordination has already been linked to lower limb injuries. Despite this, many studies fail to account for the interaction between proximal and distal joints, limiting a comprehensive understanding of joint mechanics. Indeed, the coordination between the trunk and lower limbs plays a crucial role in injury prevention, as altered trunk movement, such as increased inclination, has been associated with a higher risk of ACL injuries. Therefore, analyzing movement patterns in isolation is insufficient ; instead, a comprehensive approach considering the interdependence of body segments is necessary to fully understand joint control and injury mechanisms in sports [2].

To optimize performance while reducing injury risk, athletes must engage in both strength and power training in parallel with injury prevention programs. Sports activities, including running, jumping and sidestepping, impose significant stresses on the body. Proper neuromuscular and proprioceptive training is recommended to enhance the activation of mechanoreceptors and stabilizing muscles, particularly relevant around the ankle, allowing for early detection and response to balance loss, ultimately preventing falls and injuries [5].

Additionally, studies indicate that up to 80% of non-contact ACL injuries occur during single-leg landings and sidestepping, particularly in the weight acceptance phase, i.e. in the first 20–30% of the stance phase. This corresponds to the moment when the knee is in an extended posture ($<15^\circ$ flexion), external abduction and/or internal rotation knee moments are high, and muscle support is insufficient [3]. Fatigue further exacerbates injury risks by reducing the muscles' capacity to generate force, leading to compensatory movement patterns that alter inter-joint and inter-muscular coordination [4].

Understanding these risk factors and their interactions is essential for developing targeted training strategies that enhance performance while preventing injuries. Therefore, analyzing movement patterns independently is insufficient. Instead, a comprehensive approach considering the interdependence of body segments is necessary to fully understand joint control and injury mechanisms in sports [5]. In this context, investigating inter-joint coordination is particularly relevant as it provides insight into how movement adaptations and compensatory strategies influence joint control in response to different movement conditions, such as anticipated and unanticipated actions.

1.2 Effects of anticipation

Anticipation plays a key role in motor control and movement execution across various movements, especially jumping, cutting and landing. In controlled environments, individuals can pre-plan their movements, whereas in real-world or competitive settings, they must continuously adapt to unpredictable stimuli. This difference influences biomechanical responses and lower limb kinematics, as shown in studies comparing planned and unplanned tasks.

The anticipation effect refers to the tendency of individuals to modify their movement patterns when they expect potential threats or dangers. This concept is commonly seen in sports, where research has shown that unplanned movements tend to be riskier than planned ones. This may be due to the fact that rapid, unanticipated actions can disrupt muscle activation patterns, leading to abnormal joint kinematics. However, there is limited knowledge on whether unplanned movements affect joint stability or overall functional performance during dynamic tasks. This information would be crucial in determining whether the anticipation effect should be considered in dynamic functional assessments following ligamentous injuries [6].

In this study from Fong et al. [6], stop-jump tasks were analyzed in planned and unplanned situations. Participants were instructed to run in a straight line for 10 meters, land with their right foot on a force plate and then immediately perform a jump in one of four possible directions : left, right, forward or vertical. The difference between the planned and unplanned conditions lies in the timing at which participants are informed of the jump direction ; either before starting the trial, or only 0.7 meters before reaching the force plate, respectively. Studies comparing planned and unplanned movements have shown that unanticipated tasks lead to modifications in knee rotational stability and a decrease in knee external rotation at touchdown. This may reflect an adaptive strategy or increased joint stress, potentially increasing the risks of ACL injuries. Some research has also reported greater knee valgus and flexion moments in unplanned movements, suggesting higher joint loading. Joint loading refers to the forces and stresses applied to a joint during movement. These biomechanical adaptations likely occur during the flight phase, as individuals attempt to adjust their landing strategy in response to uncertainty. Specifically, studies on stop-jump tasks have demonstrated that anticipation significantly influences knee kinematics, particularly tibial rotation relative to the femur in the landing phase. Findings indicate that planned and unplanned stop-jump tasks result in distinct knee kinematics, reinforcing the role of anticipation in landing mechanics. Given that real-game situations involve continuous unpredictability, functional assessments should integrate unplanned tasks to better reflect competitive conditions. This is particularly relevant for rehabilitation and return-to-play evaluations, where assessing knee stability under reactive conditions is essential to reducing injury risks and ensuring safe performance.

Another interesting factor to consider is familiarity with a movement. In their study analyzing evasive maneuvers, Connor et al. [7] demonstrated that greater familiarity with a movement enhances anticipation accuracy and the ability to deal with unplanned situa-

tions. Specifically, the elite Rugby League players, who were more familiar with these evasive maneuvers, were able to anticipate the movements more accurately than the control group. This suggests that experience and familiarity with certain movements improve one's ability to react effectively to unpredictable events. In unplanned situations, such as facing unexpected action from opponents, being familiar with specific movements, allows individuals to interpret visual cues, predict outcomes and adjust actions more efficiently. This leads to better performance and helps reduce the risk of mistakes or injuries.

Moreover, a recent study from Han et al. [8] highlights how individuals with a history of ankle injuries may develop compensatory movement strategies that help them cope with unexpected perturbations. Individuals with chronic ankle instability tend to show impaired ankle kinematics, such as increased inversion and displacement, following unplanned perturbations. On the other hand, individuals known as *copers*, i.e. with history of ankle injuries but regained ankle function, display more adaptive responses. Despite a prior injury, these individuals maintain stable ankle kinematics by relying on enhanced preparatory and reactive muscle activity. Interestingly, all participants in the study, regardless of ankle condition, demonstrated increased involvement of the hip joint, particularly greater hip flexion and displacement, during unanticipated landings. This suggests that proximal joints may play a compensatory role in maintaining stability when facing sudden changes, underscoring the importance of adaptive strategies following injury.

1.3 Joint coordination

There are various definitions of joint coordination, but the one adopted here is : *Joint coordination is the spatiotemporal relationship between kinematic, kinetic and physiological variables of two or more limbs performing a motor task with a common goal* [9]. Joints, also referred to as articulations, connect bones and play a critical role in maintaining the stability of the skeletal system while allowing specialized movements.

Inter-joint coordination is crucial in complex motor tasks, particularly in sports requiring rapid and precise limb movements. Kim et al. [10] explored inter-joint coordination during Taekwondo kicks using three-dimensional kinematic analysis. They proposed a coordination index to quantify the relationship between hip and knee movements, distinguishing different movement strategies. Their findings highlighted the importance of understanding these patterns for optimizing speed and efficiency in dynamic movements, a concept highly relevant for volleyball receptions, where different conditions, i.e. planned vs. unplanned may require distinct movement strategies. This study, using 3D motion capture similar to tools like Qualisys, demonstrates how joint coordination can be modulated under various constraints.

To sum up, understanding inter-joint coordination is crucial for analyzing movement differences between planned and unplanned situations, such as those encountered during volleyball receptions, where distinct movement strategies may be required to optimize performance. Additionally, this knowledge is essential for assessing injury risks, as improper coordination patterns may increase the likelihood of musculoskeletal strain or injury.

1.4 Approaches to determine inter-joint coordination

Characterizing human movement is crucial for understanding movement disorders, comparing different situations or even assessing rehabilitation progress. Advances in motion capture technology have made it easier and more accessible to record human movement. In recent years, various methods have been developed to analyze inter-joint coordination. However, there is still no clear consensus on the most appropriate metrics for evaluating inter-joint coordination in movements based on kinematic data. So, this section aims to present the main approaches currently used and compare them.

1.4.1 Pearson correlation coefficient

In a study from Irawan et al. [11], the Pearson product-moment correlation coefficient (r) was used. It is a statistical measure used to evaluate the strength and direction of a linear relationship between two continuous variables. It is calculated using the following formulae [12] :

$$\bar{X} = \frac{1}{N}\sum_{i=1}^{N} X_i, \qquad \bar{Y} = \frac{1}{N}\sum_{i=1}^{N} Y_i, \tag{1.4.1}$$

$$r = \frac{\sum_{i=1}^{N}\big((X_i - \bar{X})(Y_i - \bar{Y})\big)}{\sqrt{\sum_{i=1}^{N}(X_i - \bar{X})^2}\sqrt{\sum_{i=1}^{N}(Y_i - \bar{Y})^2}}. \tag{1.4.2}$$

where X_i and Y_i are individual data points, and N the number of observations.

The result of this Equation 1.4.2 ranges from -1 to 1. When r = 1, there is a perfect positive correlation; when X increases, Y increases. When r = -1, we have a perfect negative correlation; when X increases, Y decreases. If r = 0, there is no linear correlation between X and Y, they move independently from each other.

As can be observed in Figure 1.1, for a correlation coefficient of zero, the points show no particular direction, are scattered, and no line fits the points on the graph. As the correlation coefficient increases, each measurement clusters more closely in a linear pattern. The line is difficult to detect when the relationship is weak (e.g., r = -0.3), but it becomes clearer as the relationship strengthens (e.g., r = -0.99).

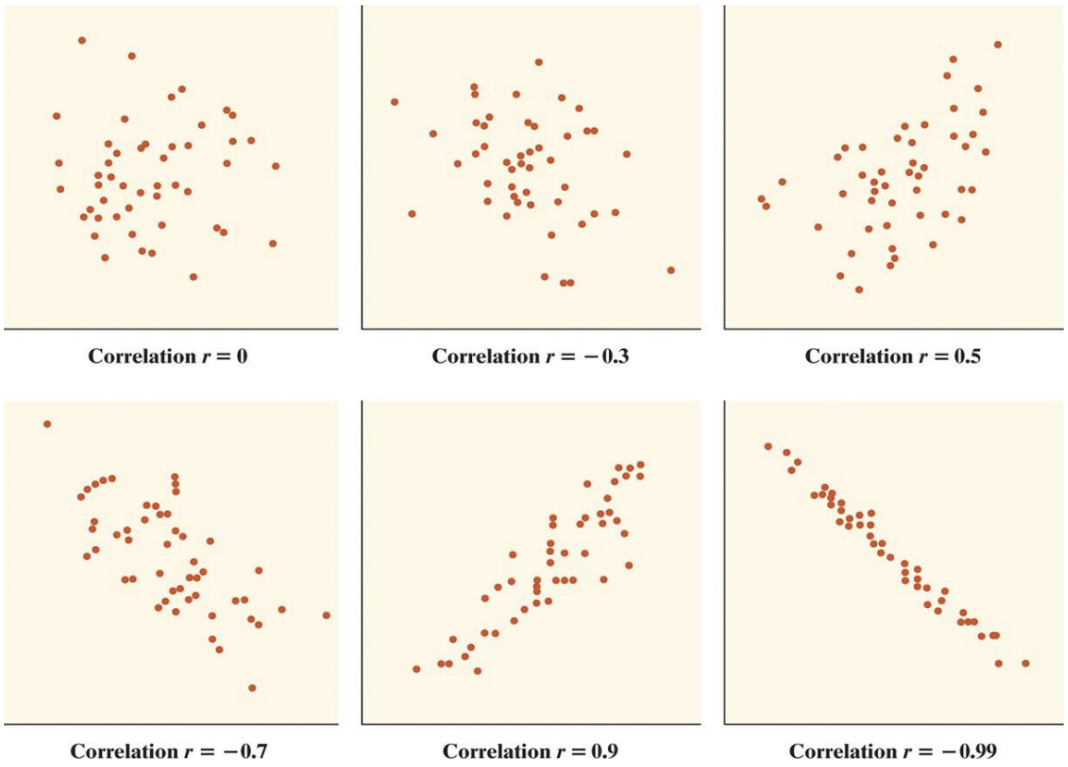

Figure 1.1: Scatter plots depicting different levels of correlation using the Pearson correlation coefficient [13].

Pearson correlation is widely used in various scientific fields, including biomechanics and joint coordination research. In joint coordination analysis, it helps determine whether two joint angles or angular velocities move in a synchronized manner. For instance, it can assess the coordination between the hip and knee during landing or analyze the interaction of lower limb joints in gait studies.

However, Pearson correlation analysis has some limitations. It assumes a linear relationship between the two variables. If this relationship is nonlinear, Pearson correlation may not provide meaningful insights. It is also very sensitive to outliers. Thus few extreme values can distort the correlation, making it appear stronger or weaker than it truly is. Pearson correlation assuming a linear relationship between variables can sometimes be applied in biomechanics studies like gait or cutting maneuvers. While joint movements can show some linear coordination, especially during specific phases, the relationship may become nonlinear in more dynamic movements or at higher ranges of motion. Therefore, while Pearson's correlation can be useful, it is important to assess whether the linear assumption is appropriate for the specific joint interactions being analyzed [12, 14].

1.4.2 Continuous relative phase

Park and Yoon [15] used the continuous relative phase (CRP) method to assess inter-joint coordination. This approach enables to assess joint coordination by analyzing the phase relationship between two degrees of freedom (DFs) by measuring the difference in their phase angles over time. CRP is computed by subtracting the phase angle of the proximal DF from that of the distal DF at each time point. The coordination pattern can be further analyzed by calculating the standard deviation of CRP across all time points and trials or subjects, which represents variability. Lower CRP variability indicates more stable and consistent coordination, while higher variability suggests less consistent movement patterns. [16]

CRP is one of the most widely applied metrics. This type of analysis involves both the measured signal θ(t), which represents the displacement of segment and is time dependent, and its velocity $\dot{\theta}$(t), which is the first derivative of the signal. In this context, normalization is crucial, as it enables the comparison of signals by eliminating the effects of differences in amplitude, frequency, and offset. This makes the interpretation of phase portraits and coordination analyses more straightforward. A phase portrait is a graph that plots a variable against its first derivative, in this case, the angular displacement against the angular velocity [17].

The normalization method used depends on the nature of the signal. Given the nature of human movements, the focus will be put on non-sinusoidal signals, as is commonly assumed in similar research studies [15, 18]. In this case, the common way is to use two different equations to normalize joint angular displacement and angular velocity. The goal of normalization for both signals is to scale them to a range between -1 and 1. To normalize the joint angular displacement, the following equation is used :

$$\theta_{i\ norm}(t) = 2 \times \left(\frac{\theta_i(t) - \min\left(\theta_i(t)\right)}{\max\left(\theta_i(t)\right) - \min\left(\theta_i(t)\right)} \right) - 1 \tag{1.4.3}$$

Using Equation 1.4.3, the minimum value of the original signal becomes -1 after normalization, and the maximum value becomes 1. For angular velocity, normalization is achieved using the following equation :

$$\dot{\theta}_{i\ norm}(t) = \frac{\dot{\theta}_i(t)}{\max\left(|\dot{\theta}_i(t)|\right)} \tag{1.4.4}$$

In Equation 1.4.4, the zero value after normalization will still represent the zero value of the original signal, which is important when the zero value has a qualitative meaning. Indeed, zero value in velocity is significant as it indicates an instant when motion temporarily stops.

After normalization, the phase angle can be calculated as :

$$\phi_i(t) = \arctan\left(\frac{\dot{\theta}_{i\ norm}(t)}{\theta_{i\ norm}(t)}\right) \tag{1.4.5}$$

and CRP is expressed as :

$$CRP(t) = \phi_1 - \phi_2 \tag{1.4.6}$$

where 1 and 2 represent the proximal and distal segment respectively.

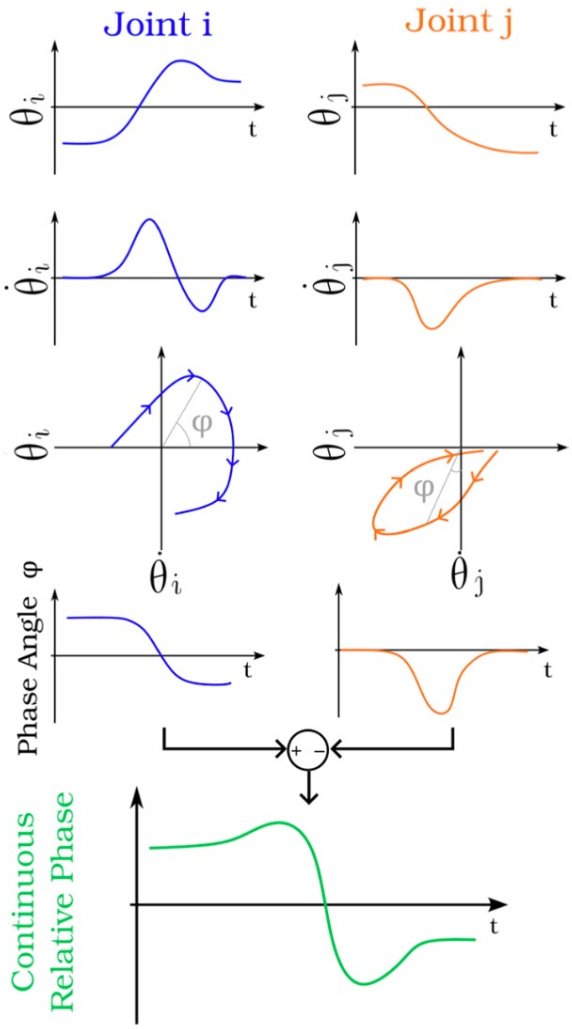

Figure 1.2: Continuous Relative Phase (CRP) Computation [15].

Figure 1.2 illustrates the process of obtaining CRP, with graphs representing each step of the computation.

About interpretation, a constant CRP indicates stable coordination, meaning that each time the movement is performed, the phase relationship between the two segments re-

mains roughly the same. On the other hand, deviations suggest that one joint is progressively shifting out of phase. This means that the movements of the segments are not always synchronized in the same way. For example, in one trial, the distal segment could precede the proximal one, and in another trial the distal could follow the proximal. This is reflected by a CRP that fluctuates significantly from one trial to another, with peaks and oscillations occurring at different times. The standard deviation of CRP quantifies this variability, with lower variability generally indicating better coordination [14].

Thus, CRP provides a continuous measure of coordination throughout the entire movement, rather than focusing on discrete events. This method allows to analyze directly the relative phase between joints, whereas other traditional approaches analyze joint angles separately. As CRP is normalized, it allows comparison that are more relevant between subjects and trials, even if the range of motion varies between these. Finally, as CRP relies on computation of angular displacement and velocity, it provides a more dynamic representation than other methods, such as angle-angle plots [18].

However, CRP method has some limitations. As it relies on angular velocity computation, which is very sensitive to noise, filtering is necessary but it can have significant effects on the results. Additionally, while lower CRP variability is often associated with better coordination, there is no standardized threshold to define what constitutes *good* or *poor* coordination, making interpretation context-dependent and quite subjective. Another limitation is that CRP describes relative coordination but does not indicate which joint is responsible for a desynchronization. This makes it difficult to isolate individual joint contributions. Finally, CRP is well-suited for analyzing simple joint pairs such as hip-knee, it may not fully capture coordination in more complex, multi-degree-of-freedom movements, such as whole-body or upper-limb tasks [19]. Indeed, this technique has limitations when dealing with non-sinusoidal movements and trials of variable lengths [2].

1.4.3 Vector coding

In order to avoid limitations of the CRP method aforementioned in Section 1.4.2, Pereira et al. [2] used the vector coding method to analyze inter-joint coordination by quantifying the relationship between two joint angles throughout the movement. Vector coding is particularly valued for its simplicity and effectiveness, especially when analyzing multiple trials of varying durations and complex, non-sinusoidal movement patterns.

First, the angular trajectories of two segments, such as hip and knee, are normalized in time. This means that the movement is rescaled so that each trial spans the same time interval (from 0% to 100% of the movement cycle). This allows for comparison of movements regardless of trial duration. They are then plotted against each other to create an angle-angle diagram. Next, the coupling angle γ is calculated by connecting consecutive points on this diagram and determining the angle of the resulting vector relative to the horizontal axis. This coupling angle is obtained using the following equation :

$$\gamma_i = \arctan\left(\frac{\Delta Y_i}{\Delta X_i}\right) \tag{1.4.7}$$

where ΔY_i and ΔX_i correspond to the variation of angle between the segments for each instant i.

This provides a time series of coupling angles, which are then plotted against the normalized movement cycle, i.e. 0-100% of the movement duration. Finally, these values are categorized into four coordination modes. In-phase coordination mode occurs when both joints change simultaneously in the same direction with equal contributions, while anti-phase coordination mode occurs when both joints change at the same time but in opposite directions. In the dominant joint 1 coordination mode, only joint 1 moves. Inversely, with joint 2 remaining stationary, and in the dominant joint 2 coordination mode, only joint 2 moves, with joint 1 remaining stationary. These modes allow for the quantification of coordination patterns and their variability across different conditions. This approach is particularly useful for comparing trials of variable duration and analyzing adaptations in joint coordination under different experimental constraints, such as fatigue or unplanned movements, which can affect movement patterns or coordination strategies [2].

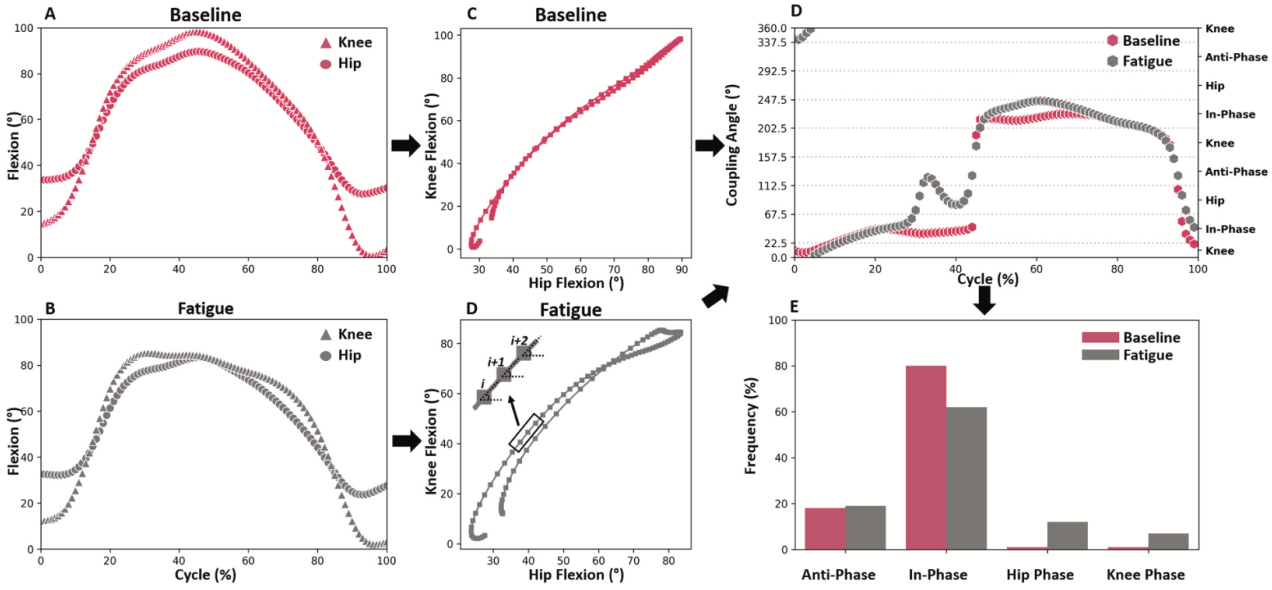

Figure 1.3: Schematic overview of vector coding technique [2].

However, even though this method is quite intuitive, easy to interpret and enables to detect differences in movement strategy, it also has some limitations. Vector coding relies on discretization of data by computing coupling angles at specific time points, which may lead to reduced precision by missing small variations compared to continuous methods like continuous relative phase. Additionally, the classification of coupling angles into different coordination

modes depends on arbitrary thresholds which decreases the reproducibility and precision, particularly when the thresholds are not suited to the specific movement being studied. Furthermore, this method may lose sensitivity to progressive transitions between coordination modes, which is critical for understanding more complex and dynamic movements.

1.4.4 Angle-angle plots and cyclograms

Angle-angle plots, also known as cyclograms when applied to cyclic movements, are graphical representations that illustrate the coordination between two joints by plotting the angle of one joint as a function of another. These plots eliminate the influence of temporal variations between individuals and trials, providing a clearer understanding of inter-joint coordination.

Harrison et al. [20] used angle-angle plots to analyze joint coordination during vertical jumps. Their findings indicated that more advanced jumping techniques are characterized by a knee-hip coordination pattern involving greater knee flexion while maintaining less hip flexion. This method allows for the examination of movement strategies independent of timing variations, making it particularly useful for assessing skill levels and movement efficiency.

Cyclograms, a specific form of angle-angle plots, are commonly employed in the study of cyclic movements such as gait analysis. Park et al. [21] investigated the impact of knee osteoarthritis on inter-joint coordination using hip-knee cyclograms. They examined various cyclogram parameters, including range of motion, center of mass, perimeter, and area of the closed-loop curve. Changes in both joints result in perimeter variations within the angle-angle diagram, reflecting alterations in movement coordination. If one joint exhibits uncoordinated motion, the perimeter of the cyclogram increases, whereas the total movement area may remain relatively stable. Additionally, perimeter variations can indicate robotic-like gait patterns, where one joint remains relatively fixed while the other rotates. The use of cyclograms extends beyond hip-knee coordination, as multiple angle-angle diagrams can be employed to assess movement patterns across the lower limb, such as hip-knee and knee-ankle coordination [22]. This approach enables both quantitative analysis, through range of motion and perimeter calculations, and qualitative assessments through the visual inspection of cyclogram shapes.

Figures 1.4 and 1.5 are examples of cyclograms that can be obtained, plotting the knee angle against hip angle [22]. Significant differences can be observed between healthy control group and patient suffering from multiple sclerosis, in terms of cyclogram shape, size, perimeter value...

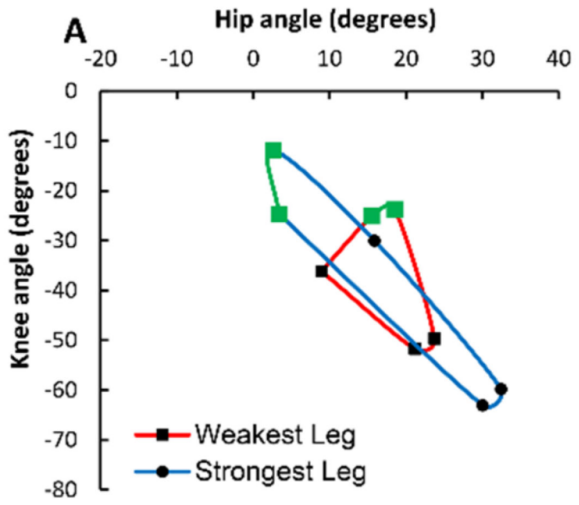

Figure 1.4: Hip-knee cyclogram of person with multiple sclerosis.

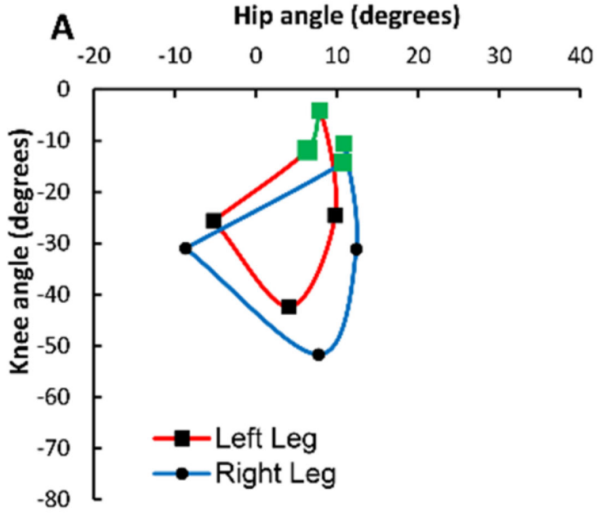

Figure 1.5: Hip-knee cyclogram of healthy person.

Cyclograms are particularly useful for detecting changes in coordination and assessing movement variability. Moreover, it is quite easy to implement. However, they are primarily qualitative and require complementary metrics for a more objective analysis. To strengthen the interpretation, additional measures such as joint torque or coordination indices (e.g., phase relative index) could be considered.

The application of angle-angle plots and cyclograms in biomechanical studies provides valuable insights into movement coordination, facilitating comparisons between pathological and healthy movement patterns. Their utilization in sports and clinical research enhances our understanding of motor control strategies and adaptations in response to various conditions.

1.4.5 Principal component analysis

In their research, Cushion et al. [23] used the principal component analysis (PCA) method. It is a statistical method widely used to analyze inter-joint coordination in human movement research. The goal of this method is to extract the main components of a multi-dimensional dataset, simplifying interpretation by keeping only independent features. This technique is particularly useful in human movement analysis, where it identifies the principal relationships among joint trajectories.

PCA is performed by computing the covariance matrix of the dataset and extracting its eigenvalues and corresponding eigenvectors. Each eigenvalue represents the variance explained by its associated principal component (PC), while the eigenvector quantifies the contribution of each original variable to the component. PCA can be conducted using either the covariance matrix or the correlation matrix. The covariance matrix preserves the original scale of the data but may downweight variables with smaller ranges. The correlation matrix

standardizes the dataset (mean of 0, standard deviation of 1), ensuring equal weighting across variables [14]. In practice, this standardization is often performed explicitly before applying PCA. This preprocessing step is particularly important in biomechanics, where variables like joint angles, forces or EMG amplitudes have different magnitudes and units. Without normalization, PCA may disproportionately reflect the variables with the highest absolute variance, leading to wrong interpretations. Standardizing the data ensures that the principal components reflect true coordination patterns rather than simple differences in scale [24].

When using PCA, a key point is the dataset size. When the dataset is too small, PCA results may be unstable. Although there is no strict minimum dataset size, stability can be assessed through bootstrapping or cross-validation, by systematically removing or modifying subsets of data and recomputing PCA. If results remain consistent, PCA is considered reliable; otherwise, variability indicates potential instability, necessitating cautious interpretation [14].

PCA is particularly valuable in reducing the complex degrees of freedom of the human body into a smaller number of PCs. The selection of PCs is based on eigenvalues of the covariance matrix, with the first few PCs revealing how multiple joints coordinate during movement. A smaller number of PCs explaining the majority of variance suggests higher synchronization among joints. Additionally, the eigenvector coefficients of the first few PCs highlight key degrees of freedom (DFs) that contribute most to movement. Plotting the first few PCs provides insight into overall coordination patterns [16].

One of the primary applications of PCA is reducing dimension of the data, enabling to keep only essential spatiotemporal patterns while minimizing redundancy. This facilitates the detection of coordination patterns both within and between individuals. PCA achieves this by applying a linear transformation that maps the original dataset into a new coordinate system with orthonormal bases, where the new variables (PCs) are uncorrelated. For a dataset with p variables observed at n time points, the raw data is represented as an $n \times p$ matrix X, where columns correspond to variables and rows to observation points. PCA transformation U maps X to a new coordinate frame Z, given by $Z = X.U$ [23]. This transformation preserves the fundamental structure of the data while reducing complexity, making PCA an effective tool for analyzing joint coordination in human movement.

In Figure 1.6, a scree plot obtained using the PCA statistical method is illustrated. In this case, more than 90% of the total variance is captured by the first two principal components (PCs). This means that these components can be used to explain the main patterns of variation in the dataset. In biomechanics, the first components would likely represent the main modes of variation in joint movements or coordination patterns.

To conclude about PCA, it is a powerful tool for reducing the dimensionality of large and complex datasets while preserving essential information. It enables researchers to identify dominant patterns of variation and compare coordination strategies across different conditions or populations. In the context of biomechanics, PCA is particularly useful for analyzing joint kinematics and coordination as it can extract common movement patterns

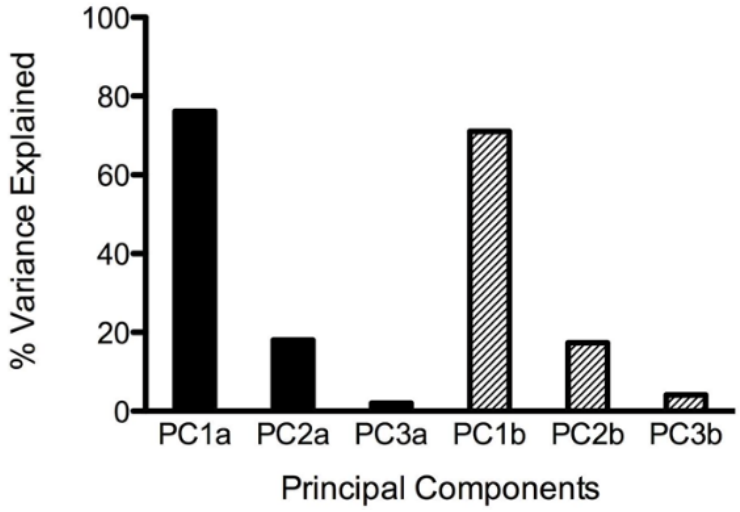

Figure 1.6: Scree plot obtained from PCA method [23].

despite inter-individual variability. Furthermore, PCA offers an advantage over methods like Non-Negative Matrix Factorization (NMF) when analyzing variables that can take both positive and negative values, such as joint angles, forces, or torques [25].

However, PCA has several limitations. It assumes linear relationships between variables, which may not always align with the nonlinear nature of motor control. The extracted components do not necessarily have direct physiological meaning, requiring careful interpretation based on experimental context and prior knowledge of biomechanics and neural mechanisms. Furthermore, while PCA can simplify data representation, it does not always provide a direct link between muscle activity and functional outcomes, making explicit modeling essential. Finally, its application in clinical settings remains challenging, as variability in motor patterns can make it difficult to draw clear conclusions without complementary analyses. Despite these limitations, PCA remains a valuable tool when used appropriately, particularly in combination with other computational and experimental approaches [25].

Chapter 2

Materials and methods

This second chapter offers a comprehensive overview of how the study's data were collected, processed and analyzed. It starts by providing a thorough description of the experimental protocol, detailing participant information, instrumentation and sensor placement, as well as the overall laboratory setup. System calibration and each stage of the experimental procedure are outlined step-by-step. This chapter then explains the processing of motion-capture data, highlighting the key preprocessing steps performed with specific softwares such as Qualisys Track Manager, Visual3D and Python. Finally, it describes the methods used to analyze inter-joint coordination, i.e. principal component analysis coupled with one-dimensional statistical parametric mapping.

2.1 Protocol

2.1.1 Aims of the study

This study aims to collect motion capture data using an optoelectronic system, along with ground reaction forces via force plates and muscle activation signals using electromyography (EMG) sensors. The optical data will then be processed using inverse kinematics techniques in Visual3D to compute joint kinematics. These kinematic outputs will be used to extract joint coordination patterns, which will be compared across different experimental conditions.

This study was approved by the Hospital-Faculty Ethics Committee of the University of Liège. Before testing, the study's objectives and experimental procedures were explained to the participants, who then provided written informed consent.

2.1.2 Participants

The sample in this study consisted in 20 volleyball players, 10 males and 10 females, from an advanced to a professional level (N3 to League A in Belgium). This selection ensures that participants have the technical expertise required for competitive volleyball, making their block performance representative of high-level play and ensuring a sufficient proficiency in the block movement. They are aged 22.4 ± 2,64 years, with a height of 180,65 ± 10,33 cm and a weight of 74,57 ± 8,14 kg. The usual frequency of training ranges from 3 to 7 days a week (4.4 ± 1,27 days/week). The least experienced volleyball player has been playing for 6 years, while the most experienced has been playing for 20 years, with an average of 14.3 ± 3,28 years. These subjects were recruited based on the following inclusion criteria : being over 18 years old and competing at a level of at least N3 in Belgium, which corresponds to playing at the national level. About the exclusion criteria, the subjects should not have had lower limb injuries in the 6 past months such as ankle sprain, fracture, Anterior Cruciate Ligament (ACL) injury... Moreover, they should not have experienced any pain in the two weeks preceding the test.

The total sample size was determined using a power analysis conducted with G*Power software. A power analysis for a paired-samples t-test (Means, differences between two dependent means) was performed, considering a medium effect size (0.5), a significance level $\alpha = 0.05$, and a statistical power $(1 - \beta) = 0.8$. Since the study compares two conditions, planned versus unplanned, without a clear directional hypothesis, a two-tailed test was used. Based on these parameters, the required number of participants was estimated at 34. To account for potential data exclusions or dropouts, an oversampling strategy was applied, leading to the recruitment of 40 participants in total. These participants were recruited through several methods : word of mouth and flyers in sports hall. In the context of this master's thesis, only 20 participants were tested, which is below the initially targeted sample size. Additional testing could be undertaken as part of future work to enhance statistical power and validate the observed trends.

The participants were asked to wear fitted clothing (a pair of shorts and a short-sleeve shirt or brassiere) to avoid any artifacts from the sensors. Indeed, the sensors are subjected to soft tissue artifacts (STA), which occur, for example, because of the relative motion between the clothing-mounted markers and the underlying bone. Thus, in this case, ill-fitting clothing can amplify this issue, leading to inaccurate measurements of motion. The subjects wore their usual sports shoes to avoid any disturbance from a change in habits. Any reflective surface was covered with tape to prevent any interference with the markers. Indeed, the system relies on the reflection of infrared light by the markers. So any additional reflective surfaces could interfere with the system's function, which is not intended. Lastly, participants with long hair were asked to tie it back in a way that left their neck exposed, ensuring all markers remained visible throughout the entire movement.

2.1.3 Instrumentation and equipment placement

The three-dimensional motion capture was performed using the QTM Qualisys opto-electronic system with a sampling frequency of 200 Hz. This system consists in 11 cameras (Arqus A9, Qualisys, Sweden). An additional camera (Miqus, Qualisys, Sweden) is positioned to capture images of the force plates, allowing for post-analysis of foot placement. To accurately track limb motion, 46 markers were placed on specific landmarks. Some markers are anatomical, positioned using palpation procedures. Others are technical, placed arbitrarily in the sense that their exact location may vary between subjects, unlike anatomical markers. Technical markers are positioned where soft tissue will have the smallest possible influence, ensuring accurate motion tracking while anatomical markers provide reproducibility and obtention of results in a reference frame with a clinical meaning. Some markers can also be called hybrid, serving both anatomical and technical purposes. The aforementioned instruments are shown in Figure 2.1.

Figure 2.1: Qualisys instruments used in the experiments : (a) Arqus A9, (b) Miqus and (c) reflective markers [26].

To track pelvis motion, five markers are placed on the right and left anterior superior iliac spines, right and left posterior superior iliac spines and the midpoint of the posterior iliac crest. The first four markers are hybrid, while the last one is technical. Lower limb motion is tracked using 26 markers, 13 on each leg. Among these, three are hybrid, positioned on the calcaneus and the bases of the second and fifth phalanges. Four others, placed on the lateral and medial epicondyles and the lateral and medial malleoli, are purely anatomical. The remaining six markers are technical, arranged in two sets of three : one set on the lateral thigh and the other on the lateral shin. Additionally, three hybrid markers are placed on the sternal notch and the spinous processes of C7 and T8 vertebrae. The last 12 markers track the motion of the upper limbs, i.e shoulders, arms and hands. Each arm has six markers positioned on the center of the medial border of the acromion process, 5 cm above the lateral epicondyle, the lateral and medial epicondyles, and the ulnar and radial styloid processes. All are hybrid markers except the one placed 5 cm above the lateral epicondyle. Figures 2.2 and 2.3 illustrate the physical placement of the markers on the body, as well as their corresponding 3D representation.

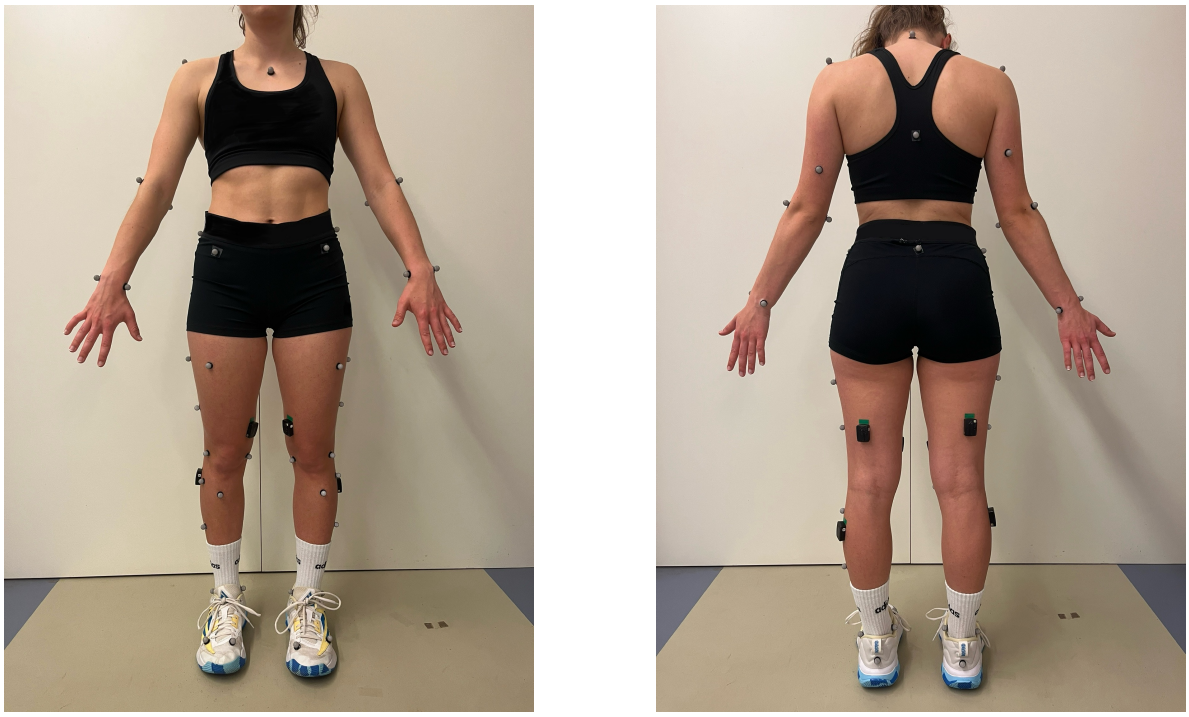

Figure 2.2: Placement of the 46 markers and 6 EMGs on a volunteer.

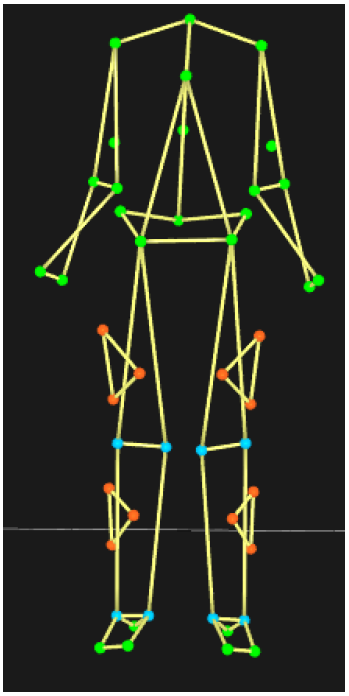

Figure 2.3: Image from Qualisys depicting the placement of the 46 anatomical (blue), technical (orange) and hybrid (green) reflective markers.

Additionally, two force platforms (9281EA, 60x40 cm, Kistler, Switzerland) were used to capture the Ground Reaction Forces (GRF) during the landing phase of the block action at a sampling frequency of 1,000 Hz. These force plates are embedded into the floor. Figure 2.4 illustrates the force plates used in the experiment.

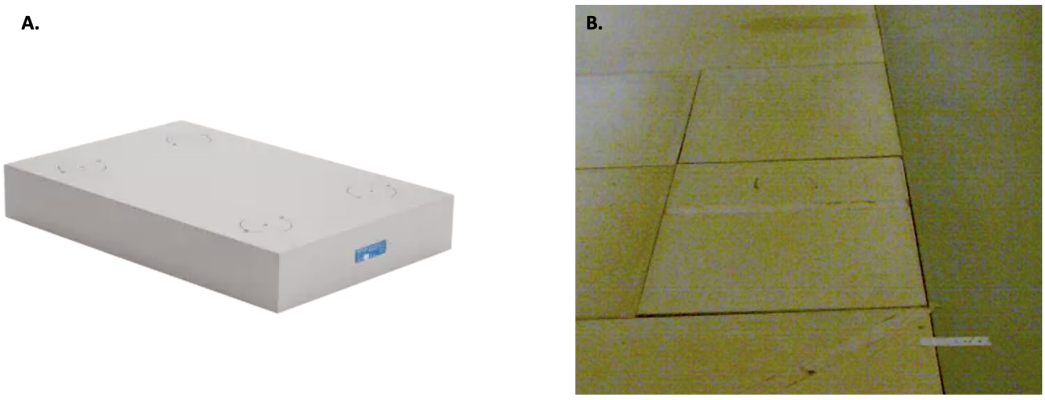

Figure 2.4: Kistler force plates: (a) image from the manufacturer's website [27], and (b) placement in the Human Movement Analysis laboratory.

Finally, six Electromyography (EMG) sensors (Trigno Avanti Sensors, Delsys, USA) were used to acquire data about muscle contraction with a sampling frequency of 1,000 Hz. These sensors were placed on vastus medialis, biceps femoris and lateral gastrocnemius of each leg. Their placement is shown in Figure 2.2, and the sensor itself is depicted in Figure 2.5.

Figure 2.5: Trigno Avanti EMG sensor from Delsys [28].

2.1.4 Experimental setup

The experimental setup was designed to closely reproduce a real volleyball game situation. This approach ensures that the collected data is as realistic as possible, leading to more relevant conclusions.

First, a badminton net is attached to two vertical posts, one on each side, to simulate a volleyball net and poles. It is placed at a height of 2.43 meters for males and 2.24 meters for females, as both genders do not play with the net at the same height in official games. The two vertical posts are separated by seven meters. Afterwards, two long sticks are placed, one at each extremity. These sticks are only useful as a visual target. They aim at encouraging the subjects to jump as high as possible and represent the opponent in a real game situation. These are placed just behind the net, closely simulating reality, where the ball typically passes near the net band. The external sticks are separated by a distance of 3.5 meters from the center, on each side. In the middle, a small plastic post is placed to indicate the starting point of each trial. Finally, the two force plates are positioned in front of the stick on the right extremity. They are placed so that the subjects are most likely to land with one foot on each plate, as centered as possible. The optimal position was to align the plates with their width parallel to the length of the foot, allowing for more lateral uncertainty in the landing position compared to the anterior-posterior axis. Hereafter in Figure 2.6 is depicted the experimental setup previously described in this section.

Figure 2.6: Illustration of the experimental setup implemented in the Human Movement Analysis laboratory at the University of Liège.

2.1.5 System calibration

Before performing the experimental trials and collecting motion data related to the block action, a calibration procedure is required. Specifically, the cameras and optoelectronic markers must be carefully calibrated to ensure accurate motion capture. This process involves precisely defining the spatial positions of the cameras relative to each other and to the force plates, allowing accurate reconstruction of the three-dimensional motion data [29]. This is performed using a calibration kit from Qualisys, the same company that manufactures the cameras. The kit is illustrated in Figure 2.7.

Figure 2.7: Calibration kit from Qualisys [26].

The anatomical reference frame/markers, based on the anatomical axis of the bones, is important for repeatability and allows comparison between subjects. However, locating anatomical landmarks precisely is not always straightforward. This can negatively impact the definition of the anatomical reference frame, reduce repeatability and hinder accurate interpretation of the movement. The main sources of errors include the non-punctual size of the landmark, variable soft tissue thickness between the bone and the skin marker or even inaccuracies in the palpation procedure [29].

Additionally, skin-mounted markers placed on anatomical landmarks are often affected by soft tissue artifacts (STAs). Factors such as inertial effects, skin deformation, and relative movement between skin and bone can distort the tracking of the underlying bone. As a result, significant errors may occur. To reduce these errors, technical markers are placed at locations that are consistently visible and less affected by soft tissue motion. These markers do not align with anatomical landmarks and can vary slightly from one subject to another. They are positioned where soft tissue interference is minimal [29].

The motion of a body segment is then described using a technical reference frame defined by at least three non-collinear markers. During the calibration phase, the position of the anatomical frame is identified relative to this technical frame. This relationship is saved

as a transformation matrix, which is then applied throughout the recording to compute the anatomical frame's position from the motion of the technical markers at each time step of the movement [29]. This whole process can be illustrated by the schematic depicted in Figure 2.8.

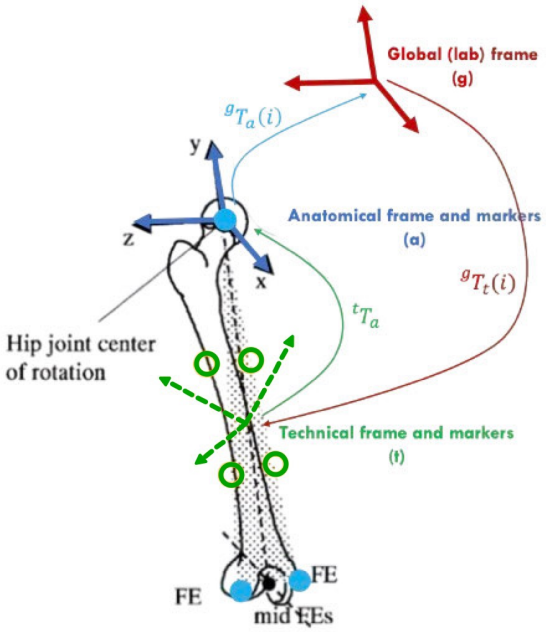

Figure 2.8: Representation of the process to express the position in the anatomical reference frame for the motion acquisition in the technical reference frame [29].

2.1.6 Experimental procedure

Markers and EMG sensors are placed as described in Section 2.1.3. Then, subjects are given 10 minutes to warm up, as they would usually do before a training or a game. They are also invited to walk freely on the camera or test the set up to conform with the laboratory environment. They are allowed to perform several attempts as a training before the real recording.

Afterwards, three maximal isometric contractions are asked for each muscle of interest. Maximal knee extension and flexion are performed to capture the activation of the vastus medialis and biceps femoris, respectively. To assess the activation of the lateral gastrocnemius, participants were instructed to perform a maximal plantar flexion by standing on their toes and contracting the muscle. These maximal contractions are illustrated in Figure 2.9, which shows how each was performed. These recordings are essential for normalizing the EMG signals prior to analyzing muscle activation.

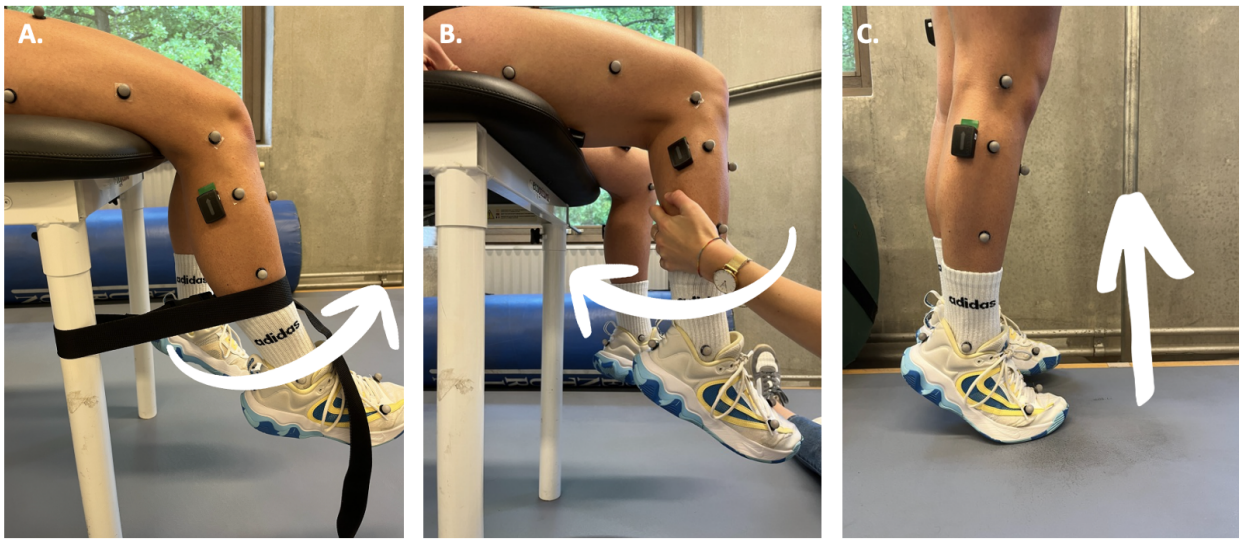

Figure 2.9: Illustration of the three maximal isometric contractions used for EMG normalization : (a) knee extension, (b) knee flexion and (c) plantar flexion.

Subsequently, a static acquisition is carried out for calibration. The subject is just asked to stand in a natural position, palms facing forward. The static acquisition is used to relate the technical markers to the anatomical ones, as described in the previous Section 2.1.5. Thereafter, the subject can start the actual testing. The participants are asked to perform a blocking action as they would in real game situation. To ensure consistency, they are asked to perform a three-step block and reach the net as quickly as possible. Participants are subjected to two different situations : planned and unplanned. In the planned condition, they know in advance on which side they must execute the block. This allows them to foresee their movement without time pressure. However, once the movement is initiated, they must execute it explosively to reach the target quickly. In the unplanned condition, as soon as they receive the cue from the operator, they must react rapidly. This does not give any room for reflection, anticipation or conscious planning. The unplanned situation is replicated by using a loud oral signal, either *Left* or *Right*. After landing, participants must take an opening step, simulating a quick transition from blocking and landing to attack preparation. This blocking action described above and performed during testing is shown in six sequential frames in Figures 2.10 and 2.11.

To consider the trials as valid, several conditions must be met. First, the correct side must be taken. Then, most specifically in the unplanned situation, the reaction and movement speed must be as fast as possible. Finally, upon landing, exactly one foot must be placed on each force plate. Additionally, both feet must be entirely on their respective force plate, without overlapping the ground or the other plate. Furthermore, the subject must land in a balanced position. Any trial that does not meet these requirements must be excluded.

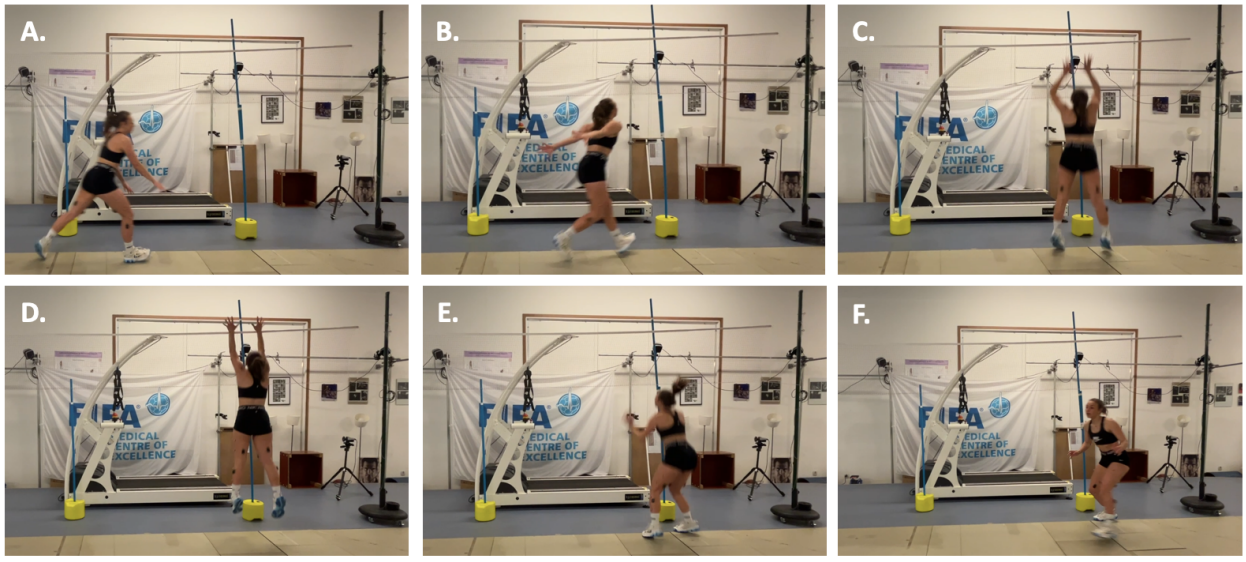

Figure 2.10: Six frames depicting different stages of the block movement illustrating the progression of the motion.

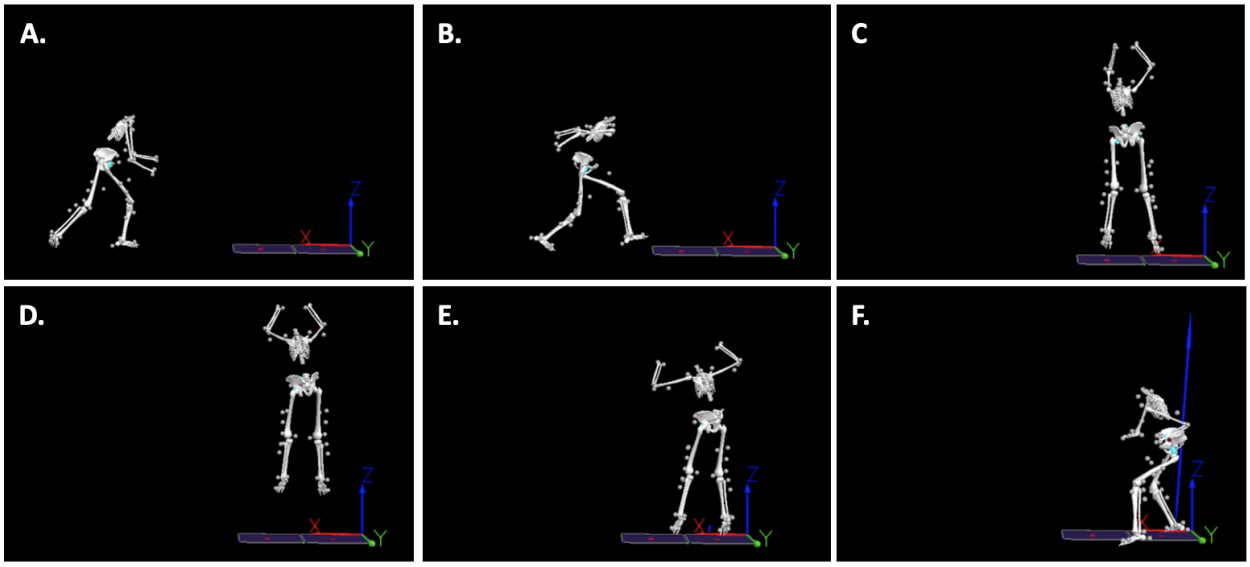

Figure 2.11: Six frames depicting different stages of the block movement, visualized through the Visual3D model, illustrating the progression of the motion.

One blocking action is considered as one trial. Three successful jump-landing tasks are recorded for the planned situation and in each direction. For the unplanned situation, eight trials are recorded to maintain uncertainty while ensuring that at least three trials are obtained for each direction. Indeed, if only six trials were recorded, by the sixth one, participants might anticipate the direction, as they would have already completed three trials on one side but only two on the other. Between each trial, they are given between one and two minutes rest. The participants assisted only once to the study for a session of around one hour.

2.2 Data processing

2.2.1 Processing with Qualisys Track Manager

The first stage of data processing is conducted using Qualisys Track Manager, a motion capture software designed for real-time 3D data collection through infrared cameras and reflective markers. In addition to supporting the acquisition and recording of motion data, this software also enables initial pre-processing. One of the key steps involves labeling, which consists in assigning each marker to its corresponding anatomical point label. Although this process can be automated, it is not always reliable or accurate, thus requiring systematic checking. Moreover, missing markers sometimes occur and must be reconstructed using interpolation techniques to ensure continuous data throughout the entire part of interest in the motion. For short gaps, polynomial interpolation is typically applied to smoothly bridge the trajectory. When gaps appear at the beginning or end of a movement, or when polynomial interpolation is not sufficient, relational interpolation is applied instead. This method reconstructs the marker's trajectory based on the motion of adjacent markers, assuming that the selected cluster behaves as a rigid body [30]. Once all marker trajectories are fully reconstructed, the data is exported in C3D format for further analysis in Visual3D.

Note that, during the testing phase, it was observed that marker visibility was poor for left-side blocks. This was confirmed during post-processing, where the tracking quality proved insufficient due to frequent marker loss. As a result, left-side blocks were excluded from the analysis due to this insufficient marker trajectory tracking. This issue originated from the net's positioning, which had to be aligned based on the placement of the force plates. As a result, the starting position was slightly off-center, causing left-side blocks to occur near the edge of the camera capture volume, thereby compromising both marker visibility and tracking accuracy. Therefore, the analysis focused on the right side, where both motion tracking and ground reaction force data were reliable.

2.2.2 Processing with Visual3D

The C3D files, obtained as described in the previous section, allow for further post-processing using Visual3D. The first step involves building a scaling model that is applied to each motion file. This model automatically generates the rigid body segments of interest, namely the feet, tibias, femurs, pelvis and trunk, for each trial. The scaling process is based on anatomical landmarks obtained during each participant's static trial. Additionally, the segments in the model are connected through joint constraints, ensuring that the movement of one segment depends on the others, while remaining within the natural limits of joint motion.

Subsequently, several post-processing steps are executed via a script applied to each motion file. The first step consists in filtering both marker trajectories and force plate signals. Marker trajectories are filtered using a fourth-order low-pass Butterworth filter with a 12 Hz cutoff frequency. This value was selected based on a review of multiple studies involving similar tasks (e.g., landing or side-stepping), where cutoff frequencies ranged from 10 to 15 Hz. Thus, 12 Hz was chosen as a reasonable compromise [3, 31, 32, 33]. GRF signals are filtered using the same type of filter but with a 60 Hz cutoff frequency, in line with values reported in the literature [34, 35]. Once filtering is complete, the relevant kinematic data can be extracted. In this study, the extracted variables include ankle and knee joint angles in the sagittal plane, and hip and trunk angles in all three anatomical planes, transverse, frontal and sagittal.

Finally, prior to exporting the data, the start and end points of each trial must be defined. The start of the motion is identified as the moment when the sum of vertical GRF from both force plates exceeds 20 N, marking the landing event. The end point is defined as the moment when the vertical force on the left force plate drops below 10 N, indicating that the left foot has left the ground. All relevant data are then exported as .txt files for each trial and participant.

2.2.3 Processing in Python

The motion data, i.e. the evolution of joint angles over time, were processed in Python to apply various methods of inter-joint coordination analysis. As a preliminary step, all datasets were time-normalized to ensure comparability across trials.

Principal component analysis

A first method used to assess inter-joint coordination is Principal Component Analysis (PCA). In this analysis, PCA was applied to matrices where each column represented a joint angle and each row a time point in the normalized movement cycle. Four separate PCAs were performed on matrices representing the mean of all trials within each group : planned, unplanned, male and female. This allowed for direct comparisons of coordination patterns between planned vs. unplanned and male vs. female conditions.

Prior to applying PCA, each mean matrix was standardized using the `StandardScaler()` function from the scikit-learn library. This step normalized the data to have zero mean and unit variance. PCA was then carried out using the `PCA()` function, which applies singular value decomposition (SVD) to extract the principal components (PCs), the corresponding eigenvalues (explained variance) and the loading scores. The results of this analysis were presented as scree plots showing the variance explained by each PC, and heatmaps illustrating the loading coefficients, i.e. the contribution of each joint angle to the PCs. Interpretation was limited to the first four principal components, as subsequent components had negligible explanatory power and were considered non-significant.

Furthermore, the standard heatmap representing the loading scores was found to be difficult to interpret, as most joints exhibited similar loading coefficients across the principal components. To facilitate the identification of distinct groups of variables associated with each PC, the Varimax rotation method can be applied. Varimax is an orthogonal rotation technique used in PCA to enhance interpretability by redistributing the variance more evenly among the components. It does so by maximizing the sum of the variances of the squared loadings within each component, which tends to produce a solution where each variable has a high loading on only one component and near-zero loadings on the others. This results in a more sparse and interpretable structure, where each component, or synergy, is more clearly associated with a specific subset of joints. Applying Varimax rotation thus allows for a clearer qualitative interpretation of the PCs by highlighting the dominant synergies to each component. However, it is important to note that the rotated loadings are no longer the original projection coefficients of the variables onto the unrotated components. Therefore, Varimax should be used primarily for qualitative interpretation purposes, not for reconstructing the original data or performing quantitative comparisons.

SPM1D methodology

To deepen the interpretation of the results, plots of GRF or joint angles across the duration of the movement are often included. While these plots provide valuable insights, they primarily allow for visual and qualitative assessments. To address this limitation, the one-dimensional statistical parametric mapping (SPM1D) methodology is introduced. Typically, when generating these plots, mean and standard deviation values are calculated and displayed. However, statistical hypothesis testing, i.e. the process of determining whether observed differences between conditions or groups are statistically significant, is often limited to a few discrete summary measures, such as peak values or values at specific time points, rather than applied to the full time-varying data. SPM1D addresses this limitation by allowing statistical testing to be conducted directly on the full one-dimensional trajectories. Instead of comparing a single value (e.g., angle at 50% of the cycle), it compares entire curves. The method treats the data as continuous functions and applies tools from random field theory (RFT) to assess whether significant differences exist at any point along the curve. Originally developed for spatial data analysis in neuroimaging, RFT is used to account for spatial correlations and controls the family-wise error rate, i.e. probability of making one false positive. Its application to biomechanics allows for robust statistical inference across

the time domain of biomechanical signals. A key strength of statistical parametric mapping (SPM) is that statistical results are presented in the same time domain as the original data, preserving the spatiotemporal context and making interpretation more intuitive [36].

Practically, the SPM1D methodology is implemented using the `spm1d` package in Python. In this study, three statistical hypotheses are tested : planned vs. unplanned conditions, male vs. female participants and left vs. right legs. Although multiple statistical tests exist, two-sample tests were selected for this analysis. Specifically, a paired t-test was used to compare planned and unplanned situations, as well as left and right legs. These comparisons involve dependent samples, since the same individuals are measured under both conditions. In Python, the function `spm1d.stats.ttest_paired()` is used for this purpose. In contrast, to compare male and female participants, an independent two-sample t-test was used, as the groups consist in different individuals. This analysis was performed using the `spm1d.stats.ttest2()` function. According to the parameters used in the `spm1d` functions, the general line of code is:

```
t.inference(alpha=0.05, two_tailed=True, interp=True)
```

Here, `alpha` is set to 0.05, which is a common significance level. In statistics, this corresponds to accepting a 5% risk of incorrectly rejecting a true null hypothesis (Type I error). The parameter `two_tailed=True` indicates that differences can be detected in both directions, i.e. either positive or negative. Finally, `interp=True` enables interpolation between discrete points to provide a more precise estimate of significant regions, as the statistical threshold may lie between sampled points [37].

Chapter 3

Results and Discussion

This third chapter presents and interprets the findings of this study. It begins with an analysis of task planning using principal component analysis (PCA), illustrated through various graphical representations such as scree plots, heatmaps, angle–angle plots and one-dimensional plots. To support the interpretation, additional biomechanical data, including ground reaction forces (GRF), joint angle profiles, and angle-angle (AA) plots are integrated. One-dimensional statistical parametric mapping (SPM1D) is then applied to assess the significance of observed differences.

The same approach is used to examine the influence of gender on inter-joint coordination. Although gender differences were not the primary focus, preliminary observations and existing literature suggesting potential variations in movement strategies between males and females led to a secondary analysis. Therefore, the exact same data were used, but instead of being sorted into planned and unplanned groups, they were sorted into male and female groups.

All analyses were performed using Python scripts developed according to the needs of this study. These scripts handle data preprocessing, including the formatting of raw matrices exported from V3D (e.g., renaming columns, removing irrelevant rows), normalization procedures, principal component analysis (PCA), the generation of biomechanical plots (e.g., AA diagrams, joint angle profiles), and statistical testing using SPM1D. All relevant scripts are provided in Appendix 5. Results are discussed in light of previous research to highlight key insights and contextualize the findings.

3.1 Planned VS Unplanned

3.1.1 Explained variance analysis

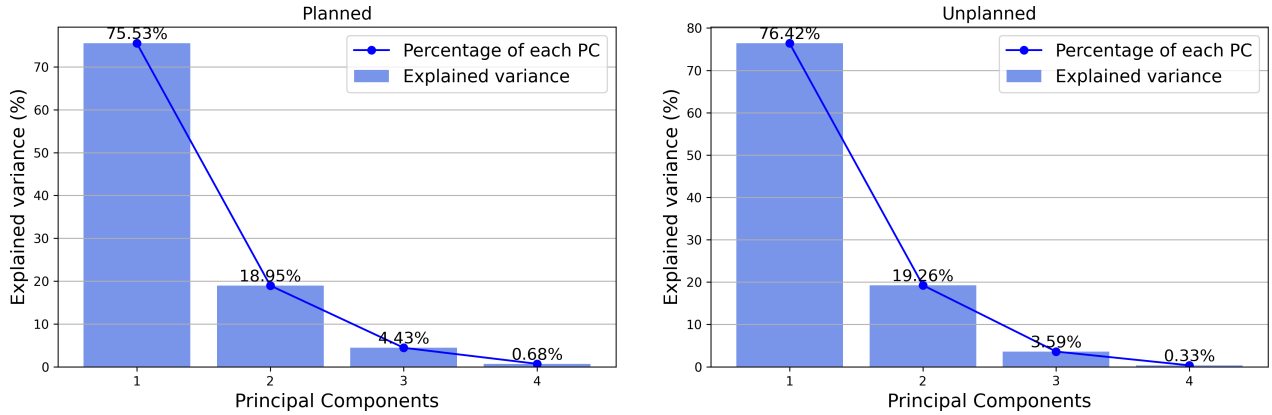

Figure 3.1: Scree plot of the explained variance for the four first PCs from the PCA analysis for planned (left) and unplanned (right) situations.

When comparing the planned and unplanned conditions, only two principal components (PCs) are needed to capture the majority of the coordination patterns, accounting for approximately 95% of the total variance in both cases. The first principal component explains significantly more variance than the second, indicating that the variables with high loadings on PC1 have a dominant influence on overall movement coordination. This trend is consistent across both conditions, with only slight differences in the proportion of variance explained. The fact that only two components are sufficient to capture most of the movement variability suggests a relatively high degree of joint synchronization. Indeed, according to Huang et al. [16], the fewer the number of components required to explain a high proportion of variance, the more coordinated the joint behavior tends to be. Consequently, the following analysis and discussion will focus on the first two PCs, as they capture the main features of the motion dynamics.

This kind of results looks consistent with previous studies. Indeed, Cushion et al. [23] also found in their research studying coordination strategies employed in vertical jumping under different task constraints (with and without arm swing) that two PCs are sufficient to describe more than 90 % of the total variance. In a so-called worst case, three PCs are required but this remains consistent with the observations previously described.

3.1.2 Interpretation of principal components using heatmap

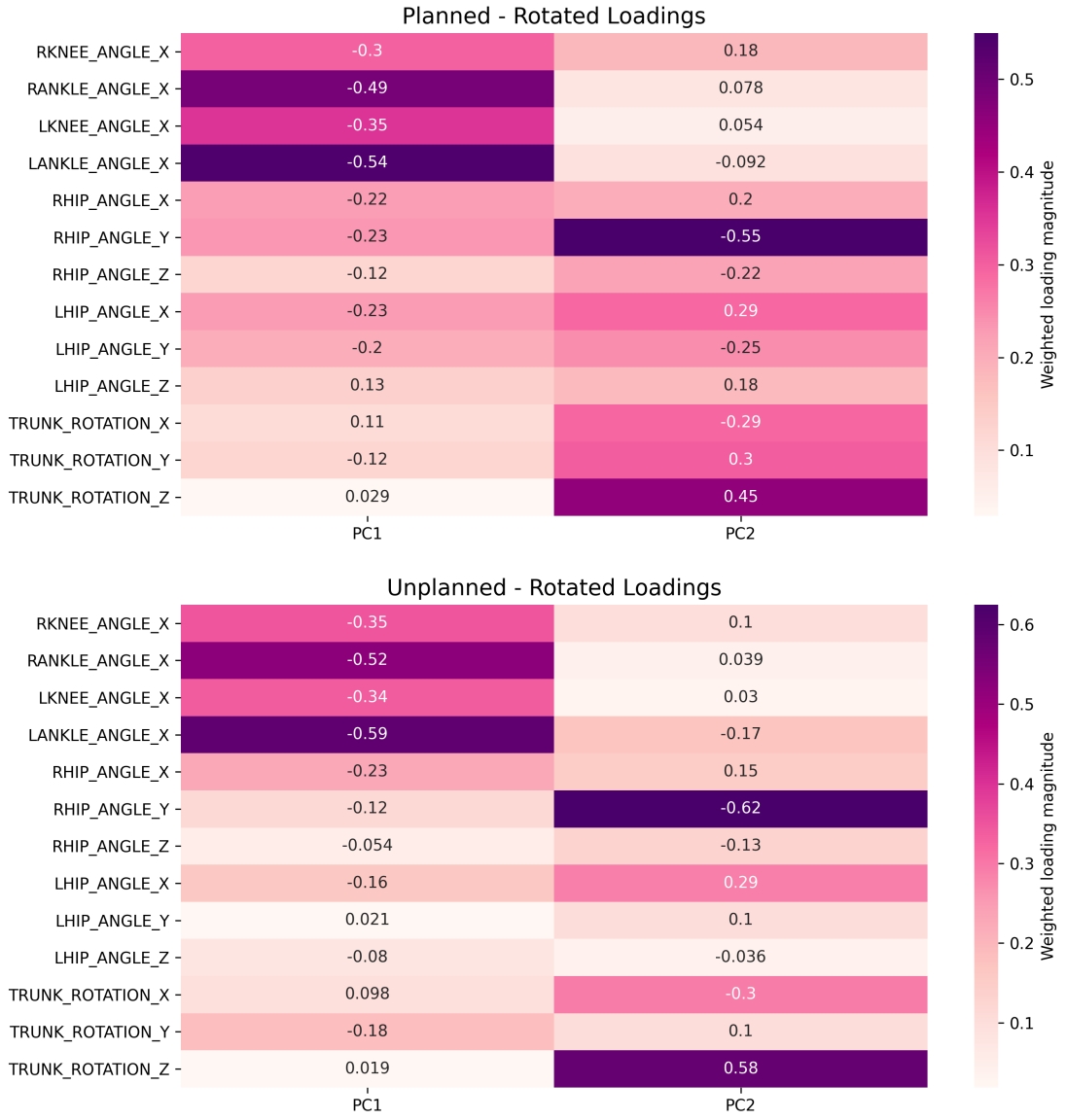

Figure 3.2: Heatmap representing the rotated loading scores of the two first PCs for planned (up) and unplanned (down) situations. The color scale is based on the absolute values of the coefficients.

The PCA was performed separately for the planned and unplanned conditions, with a Varimax rotation applied in each case to facilitate interpretation, as explained in previous Section 2.2.3. The analysis is based on the heatmaps shown in Figure 3.2. Although the components are not directly comparable between the two conditions due to the independent rotations, structural similarities can be observed.

Analyzing the first principal component (PC1), both in planned and unplanned situations, ankle angles exhibit the highest rotated loading coefficients, followed by knee angles. This indicates that the ankle and knee joints contribute most to the primary mode of movement coordination during landing. Both joints display negative loading values, suggesting they vary in the same direction. In other words, their angle variations tend to follow a similar temporal pattern : when one joint angle increases relative to the mean, the other does as well, and vice versa. These high contributions of the knee and ankle joints to the dominant pattern of variation support the idea that they play a primary role in energy absorption during landing. This observation aligns with the findings of Zhang et al. [38], who noted that at lower mechanical demands, i.e. lower landing heights, energy absorption is mainly provided by the distal muscles, notably the ankle plantar flexors and knee extensors. In the principal component analysis, the strongest contributions to the first coordination mode come from the ankle and knee angles, reinforcing the idea that these joints drive the landing strategy in this context. In contrast to higher landings, where the hip is more involved in dissipating mechanical loads, lower-height landings recruit proximal muscle groups to a lesser extent. This activation pattern allows for faster and more localized energy absorption, which may also explain why more massive but less reactive structures such as the hip extensors are less engaged. These findings underscore the critical role of precise neuromuscular regulation at the ankle and knee in managing low-impact landing tasks.

When analyzing the second principal component (PC2), the two main contributing variables are the right hip angle in the frontal plane (i.e. abduction/adduction) and the trunk rotation in the transverse plane (i.e. axial rotation). In this case, the hip angle has a negative loading while the trunk rotation has a positive loading, indicating that these two joints move in opposite directions, i.e. when one increases, the other tends to decrease, relative to their respective means. A lower PC2 score thus corresponds to increased hip abduction, i.e. greater hip angle in the frontal plane, and reduced trunk axial rotation, suggesting that the movement pattern is more influenced by hip motion than by trunk rotation. Conversely, a higher PC2 score reflects reduced hip abduction and greater axial rotation of the trunk. In this second component, a difference can be observed between the planned and unplanned conditions in the heatmap. In the planned condition, while the right hip and trunk rotation clearly dominate PC2, the other hip and trunk variables have relatively similar and lower loadings, suggesting a more balanced contribution of those segments. In contrast, in the unplanned condition, only two additional variables, left hip angle and trunk flexion/extension (sagittal plane), show some contribution, though with lower loadings. The remaining hip and trunk variables contribute even less, indicating that the coordination pattern in the unplanned situation is more narrowly focused around a few specific joint movements. According to optimal control theory discussed by Todorov and Jordan [39], motor redundancy is exploited by the motor system to optimize performance and maintain stability, even in the presence of noise or uncertainty. The results observed in the unplanned condition, with more focused joint contributions, suggest a reduction in this redundancy. This more constrained strategy could be the result of time pressure or increased cognitive load, preventing the implementation of optimal control laws, and thus compromising movement adaptability and stability.

3.1.3 Biomechanical variable analysis using SPM1D and descriptive methods

By observing the plots in Figure 3.3, the hypothesis derived from the PC1 analysis that the knee and ankle joints vary in the same direction can be confirmed. Both left and right joint pairs move in the same direction throughout the entire movement : when the knee angle increases, the ankle angle increases as well. However, small movement asymmetries are noticeable. The left lower limb appears to behave similarly in both planned and unplanned conditions. In contrast, the right lower limb shows a slightly different behavior in the unplanned condition. Specifically, in the planned condition, maximal knee flexion is greater, while maximal ankle dorsiflexion is smaller than in the unplanned condition. This may suggest that the planned condition is associated with a more cushioned landing strategy, particularly on the right side.

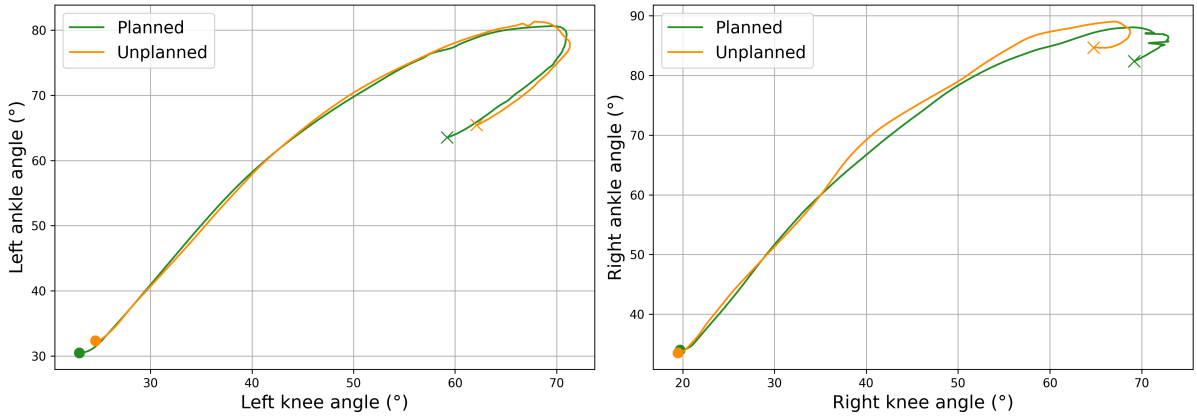

Figure 3.3: Angle-angle plots of knee and ankle joints in the sagittal plane in planned vs. unplanned situations. The landing phase starts at the dot and ends at the cross.

Differences between the left and right leg align with the task setup, as players were required to block on the right side. During the jump, they tend to "fly" in the direction of their three-step approach and land more heavily on the right foot than on the left. This is supported by Figure 3.4, which shows that vertical GRF is significantly higher on the right foot, indicating a greater vertical impact. Furthermore, the medio-lateral GRF is also larger, in absolute value, on the right foot. Interestingly, the mediolateral GRFs exhibit opposite signs for the left and right feet. Since the x-axis points towards the left, this means that the GRF on the right foot is directed to the left, whereas the GRF on the left foot is directed to the right. This can be explained by the need for compensatory mechanisms during landing to counteract the body's lateral momentum towards the right. On the right foot, this is achieved by applying force through the medial side, resulting in a reaction force directed to the left. The rightward GRF observed on the left foot, opposite to the leftward GRF observed on the right foot, may be explained by two complementary mechanisms. First, both forces being directed towards the inside of the body may reflect a strategy to stabilize the body's center of mass. Second, it is also likely that the rightward GRF on the left foot reflects the initiation of

the next movement phase, i.e. an opening step towards the left. To perform this step, the left foot pushes against the ground in the opposite direction, generating a corresponding ground reaction force. This observation is consistent with the action-reaction principle and supports the hypothesis of preparatory repositioning during the landing sequence. An additional observation is that at the end of the movement (100%), all three GRF components for the left foot are equal to zero. This corresponds to the END condition defined to determine the end of the motion, i.e. when the left foot lifts off the ground and the vertical ground reaction force measured by FP_2 falls below 10 N, as described in Section 2.2.2.

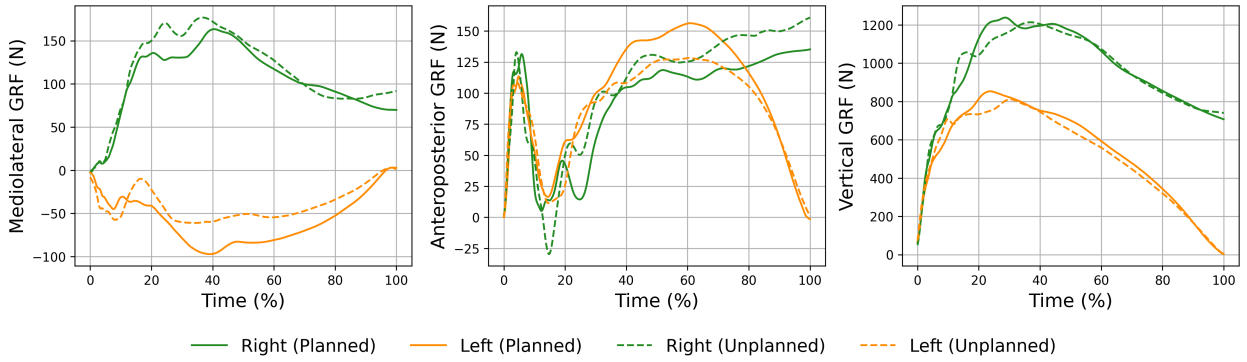

Figure 3.4: Ground reaction forces along the three spatial directions as a function of normalized time comparing planned and unplanned conditions.

Furthermore, in Figures 3.5 and 3.6, statistical analysis provides additional insight into the previously observed asymmetry. As previously noted, vertical GRFs are higher on the right foot, but this can now be discussed more precisely across the duration of the movement. Significant differences between the feet appear only from approximately 20% of the movement duration and persist until the end of the movement. The initial contact phase is then relatively symmetrical, i.e. both feet touch the ground almost simultaneously. However, as the movement progresses, asymmetry increases. This can be attributed to two main factors : the progressive transfer of body weight to the right foot, which acts as a support during the opening step, and the body's lateral momentum directed to the right. These phenomena are observed in both planned and unplanned conditions. However, in the unplanned condition, the threshold of significance is reached earlier at around 12% compared to 22% in the planned condition. This indicates that the right foot begins to bear more load sooner in the unplanned scenario. In the mediolateral direction, the difference is clearly significant throughout the entire movement, as the forces act in opposite directions for each foot. In the anteroposterior direction, no significant difference is observed until the end of the movement, which corresponds to the moment when most of the body weight is transferred onto the right foot. These observations in the mediolateral (X) and anteroposterior (Y) directions hold true for both planned and unplanned conditions.

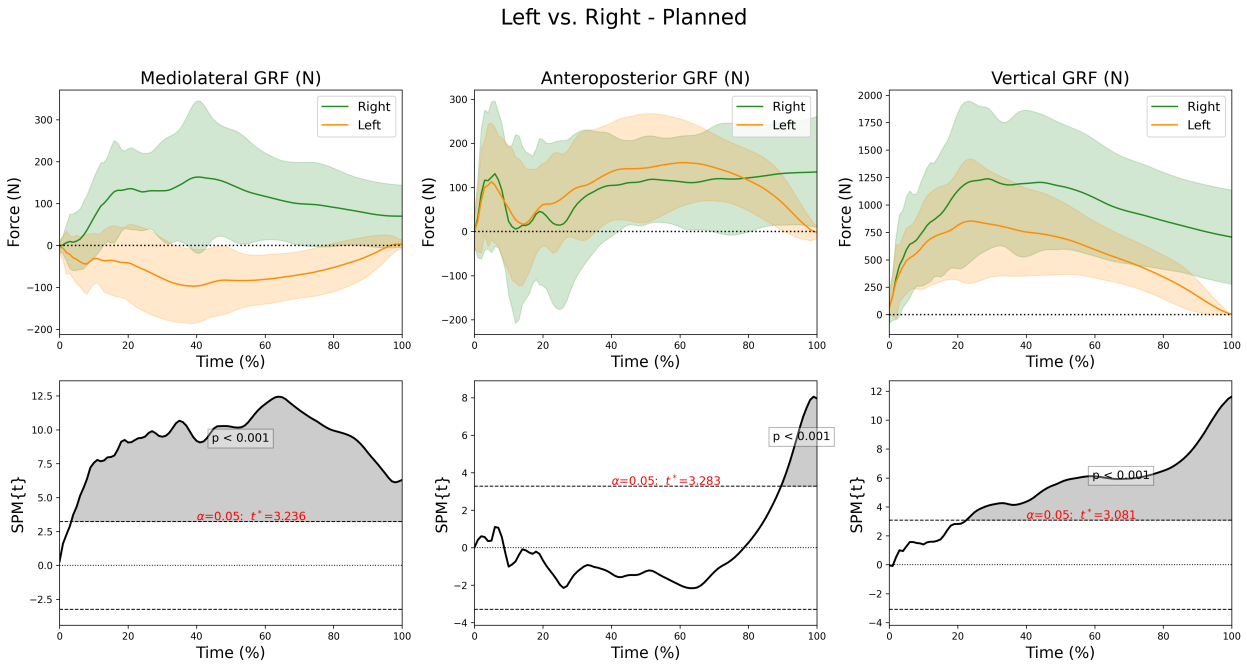

Figure 3.5: Mean GRFs in three spatial directions with standard deviation (top row). SPM1D t-test results comparing left and right feet in the planned situation (bottom row).

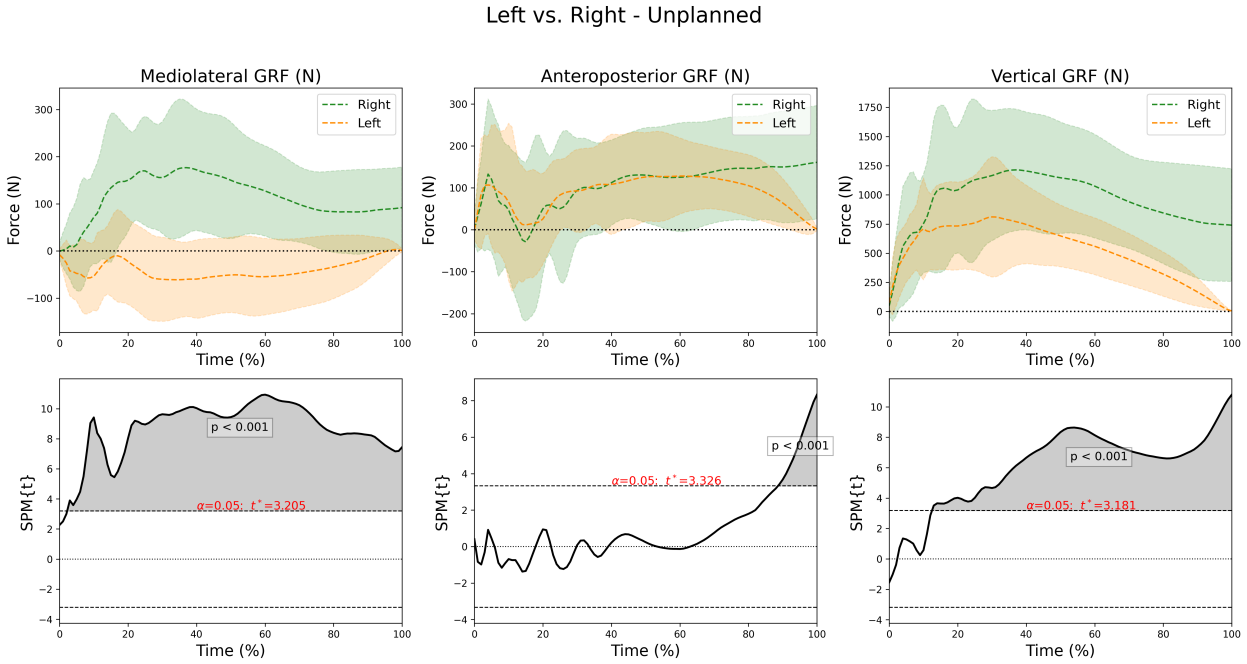

Figure 3.6: Mean GRFs in three spatial directions with standard deviation (top row). SPM1D t-test results comparing left and right feet in the unplanned situation (bottom row).

The temporal difference in load transfer between the planned and unplanned conditions may reflect an adaptation of the central nervous system to uncertainty. In the unplanned condition, the body appears to adopt a less effective anticipatory strategy, leading to a more rapid redistribution of load to the right foot. This could potentially increase the risk of overload or injury. In line with previous work on gait termination conducted by Bishop et al. [40], healthy individuals have been shown to maintain the same motor pattern across both planned and unplanned conditions, while modulating the response amplitude to meet task demands. This suggests that, when faced with unpredictability, the central nervous system may rely on an established motor program that is flexibly scaled rather than completely restructured. In addition to the timing of load transfer, the asymmetry itself between the left and right legs may have implications for mechanical stress applied to the lower limbs. Specifically, the fact that the right leg bears a higher vertical load, particularly in the unplanned condition, could increase stress on joint structures such as the knee or ankle, especially during less controlled cushioning. These findings have important implications for injury prevention, particularly regarding knee ligament damage, which is common in asymmetric jump-landing tasks.

The results of the SPM1D analysis comparing the planned and unplanned conditions are presented in Figures 3.7 and 3.8. No significant differences were found between the two conditions for either foot when considered separately. Specifically, the vertical GRF component did not differ significantly, suggesting that the unplanned nature of the movement does not substantially alter the landing strategy. For the medio-lateral GRF component, the differences were slightly more pronounced but remained non-significant.

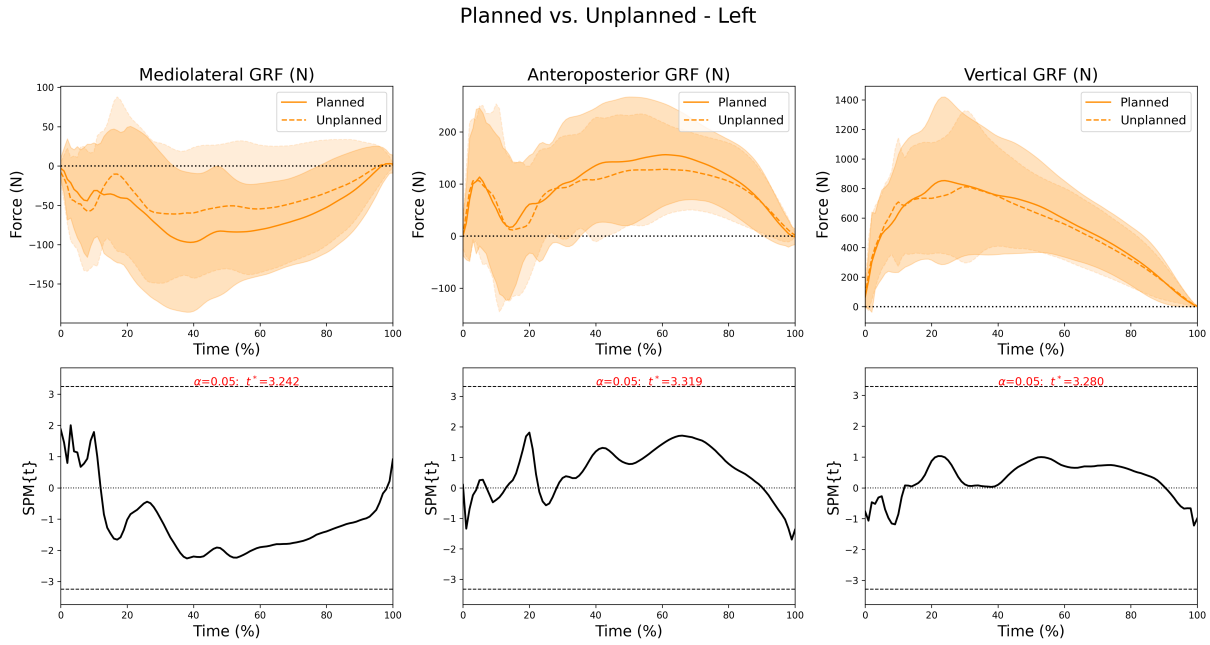

Figure 3.7: Mean GRFs in three spatial directions with standard deviation (top row). SPM1D t-test results comparing planned and unplanned situations for the left foot (bottom row).

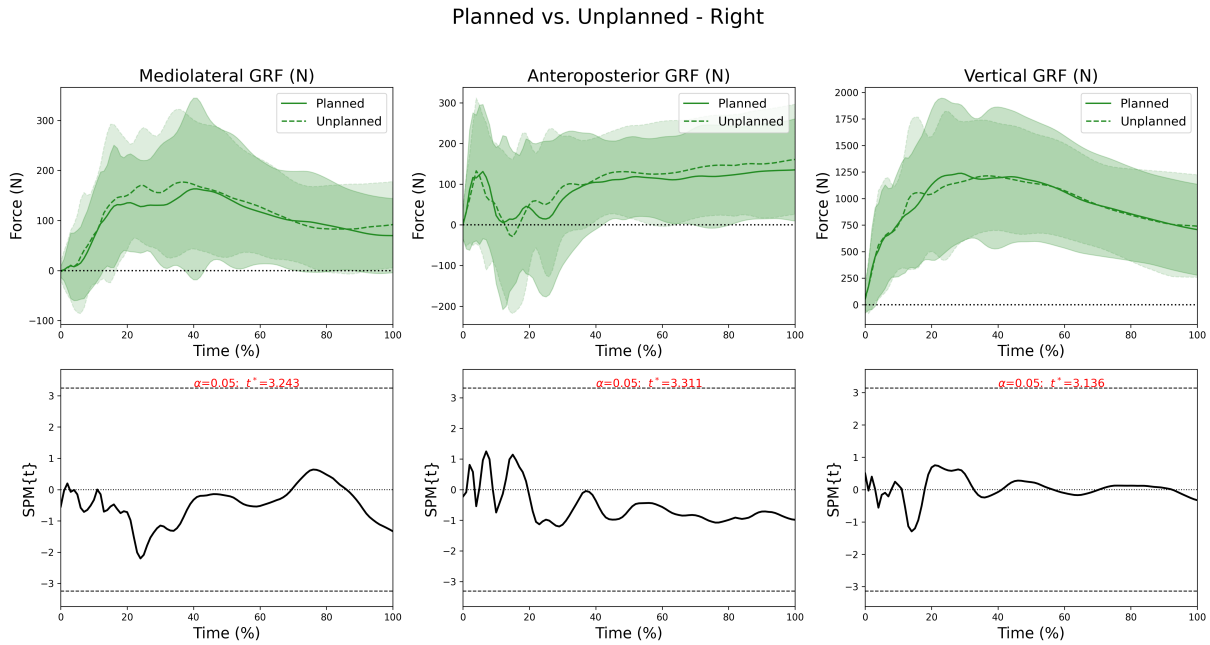

Figure 3.8: Mean GRFs in three spatial directions with standard deviation (top row). SPM1D t-test results comparing planned and unplanned situation for the right foot (bottom row).

Now that the analysis of PC1 has been completed, the subsequent analysis of PC2 is presented. The hypothesis stated previously when analyzing PC2 that right hip and trunk joints moved in opposite directions is supported by Figure 3.9, at least during the second phase of the landing. Initially, the right hip and trunk move in the same direction, both showing a decreasing angle. Then, at a certain point, while the trunk rotation angle continues to decrease, the hip angle shifts and begins to increase. The rise in right-hip angle marks the onset of abduction that precedes the post-landing steps. As detailed in Section 2.1.6, participants execute an opening step immediately after touchdown. Although one might expect the left hip, i.e. the leg that actually performs the opening step, to show the larger abduction, the movement is typically triggered by right-hip abduction coupled with trunk rotation. Regarding trunk rotation, the decreasing rotation angle during landing phase can be explained by the anticipation of the opening step and subsequent actions, as would occur in real gameplay. Participants begin rotating their trunk in preparation to these subsequent actions. As the opening step is performed, this rotation decreases, allowing them to reorient and face the game. Another observation is that trunk rotation is smaller in the planned situation compared to the unplanned one. However, this difference is not significant according to the SPM1D analysis, as shown in Figure 3.10. Therefore, no further explanation is pursued.

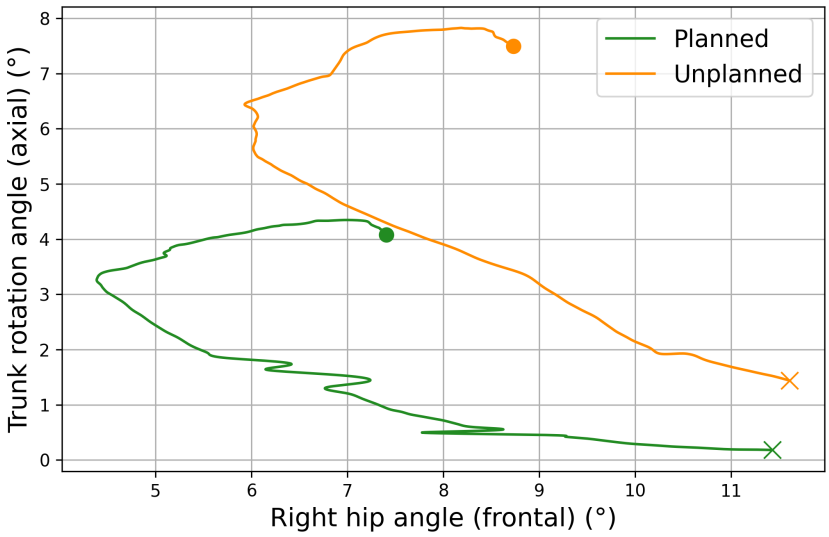

Figure 3.9: Angle-angle plot of right hip in the frontal plane and trunk axial rotation in planned vs. unplanned situations. The landing starts at the dot and ends at the cross.

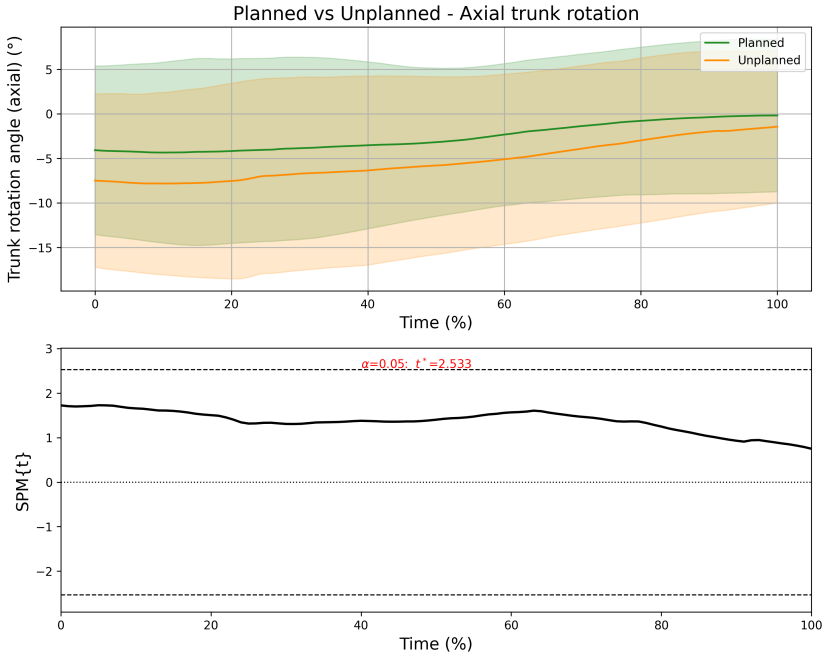

Figure 3.10: Mean trunk axial rotation with standard deviation (top) and SPM1D t-test results comparing planned and unplanned situations for trunk axial rotation (bottom).

3.1.4 Comparison with previous studies

Dennis et al. [41] investigated lower-limb kinematics during a double-limb drop-vertical jump in individuals with anterior cruciate ligament reconstruction (ACLR). Participants stepped from a 30 cm box and, upon landing, executed a maximal vertical jump. Although this protocol differs from the one employed in the present study, the respective angle-angle (AA) plots remain comparable. A comparison between the AA plots reported by Dennis et al. in Figure 3.11 and those obtained in the present study in Figures 3.12, reveals both similarities and protocol-related differences.

At initial contact, knee flexion is comparable, though slightly smaller in the current data for the right knee, indicating a marginally greater knee extension. The ankle, however, is markedly more plantar-flexed in the present study. These discrepancies can be attributed to the landing tasks. Dennis et al. asked participants to step off a 30 cm platform, leaving little time for substantial knee or ankle extension ; the ankle, in particular, begins near 90° while standing on the box. By contrast, our participants executed a jump-block action before landing, necessitating maximal plantar-flexion during propulsion and thus producing the larger ankle angles observed at landing. The protocols also account for the different ranges of motion. In Dennis et al., subjects landed and immediately performed a maximal vertical jump, which requires pronounced knee flexion and ankle dorsiflexion to store elastic energy for the subsequent take-off. In the present experiment, participants executed an opening step, focusing on energy absorption rather than immediate power generation, resulting in a smaller overall amplitude. Despite these task-specific differences, the general pattern of the curves remains comparable, displaying an in-phase relationship throughout the landing phase.

In another study by Mercado-Palomino et al. [42], the protocol was roughly similar to the one used in the present study. However, while their focus was on kinetics and kinematics, the present study rather emphasizes on joint coordination. Nevertheless, it is relevant to compare the findings and examine whether the conclusions regarding task planning are consistent with theirs. First, Mercado-Palomino et al. reported similar responses in joint angles. They defined the lead limb as the exterior one, which corresponds to the right limb in the present study. They observed that the trail limb exhibited greater ankle dorsiflexion. However, this conclusion contrasts with the findings of the present study, where greater dorsiflexion is observed in the right ankle in Figure 3.12, i.e., the lead limb. Furthermore, it can be noted that the difference in ankle angles between the left and right limbs was significant at initial contact and again from approximately 20% of the movement onward. On the other hand, Mercado-Palomino et al. suggested that the lead limb may be at greater risk of injury. This observation aligns with the present findings, where the lead limb, i.e. right leg, shows significantly higher GRF as well as greater ankle dorsiflexion. Thus, this may lead to a higher risk of injury.

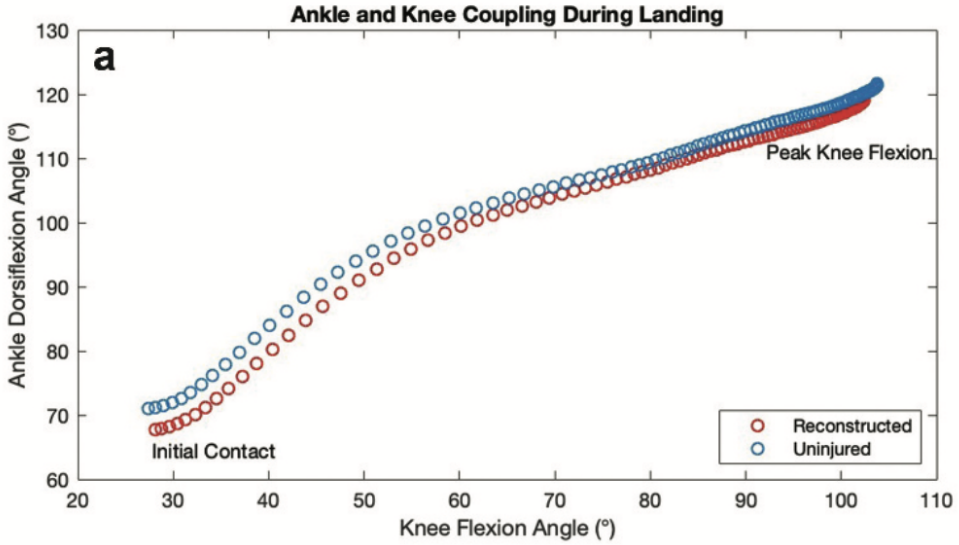

Figure 3.11: Average angle-angle plots of the (a) ankle-knee during landing and (b) knee-hip during landing [41].

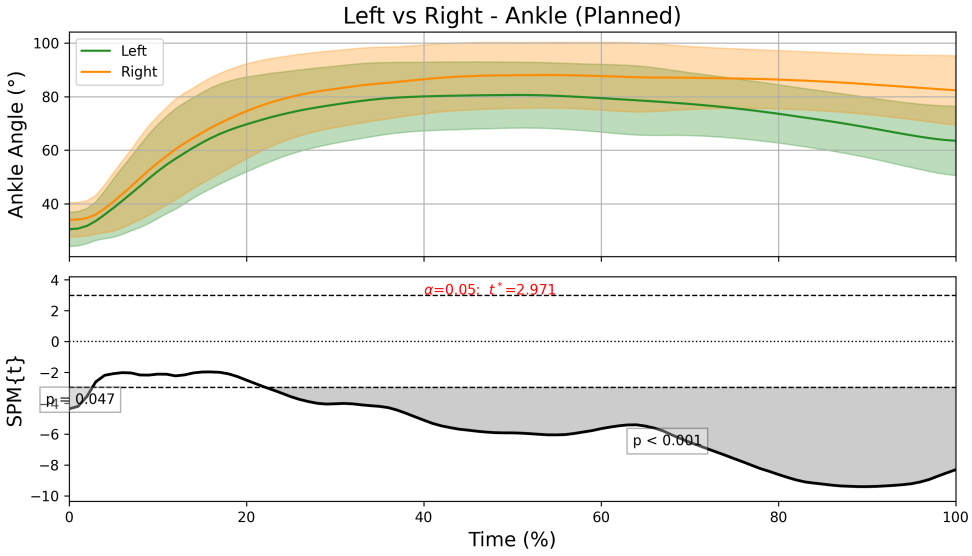

Figure 3.12: Mean ankle angle with standard deviation (top) and SPM1D t-test results comparing left and right ankle angle (bottom).

3.1.5 Effect of planning conclusion

In conclusion, the PCA did not reveal major differences between the planned and unplanned conditions in terms of joint coordination. In both situations, two components were sufficient to explain the majority of the variance, suggesting a similar overall motor control strategy. Movement was primarily governed by the distal joints, namely the ankle and knee, indicating their leading role in energy absorption during landing. The second main coordination pattern remained comparable, although a slightly more distributed contribution from hip and trunk joints was observed in the planned condition. This may reflect a more balanced segmental engagement when anticipation is possible. GRF analysis further confirmed a marked asymmetry between the lower limbs, with the right leg bearing more load during landing, a result consistent with the mechanics of a volleyball block.

Although subtle trend differences emerged between conditions, these did not consistently reach statistical significance, highlighting the robustness and adaptability of motor coordination under uncertainty. Finally, the lack of more pronounced differences may be explained by the timing of the directional instruction. As described in Section 2.1.6, the cue to block left or right was given just before the trial began. While this design choice aimed to replicate game-like conditions, it may have occurred early enough to allow participants to preprogram their landing strategies.

3.2 Male VS Female

3.2.1 Explained variance analysis

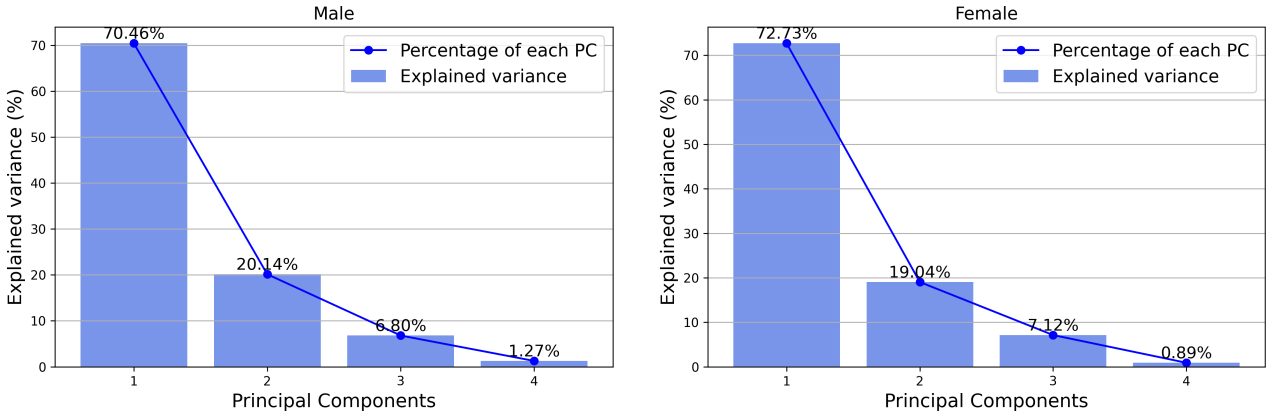

Figure 3.1: Scree plot of the explained variance for the four first PCs from the PCA analysis for male (left) and female (right).

When comparing males and females, two principal components are sufficient to explain the majority of the variance in joint motion. The low number of PCs required suggests a relatively high degree of joint coordination, similar to what was observed when comparing planned and unplanned situations. These results indicate that joint movements are strongly coupled and follow consistent coordination patterns. However, the total variance explained by the first two PCs is slightly lower, capturing around 90–92% of the total variance. The first PC still accounts for substantially more variance than the second, indicating that variables with high loadings on PC1 continue to play a major role in the movement and coordination. This trend holds true for both males and females, with minor variations in explained variance. Notably, the third principal component contributes to a slightly higher proportion of variance compared to previous comparisons, though it remains significantly lower than the first two components.

3.2.2 Interpretation of principal components using heatmap

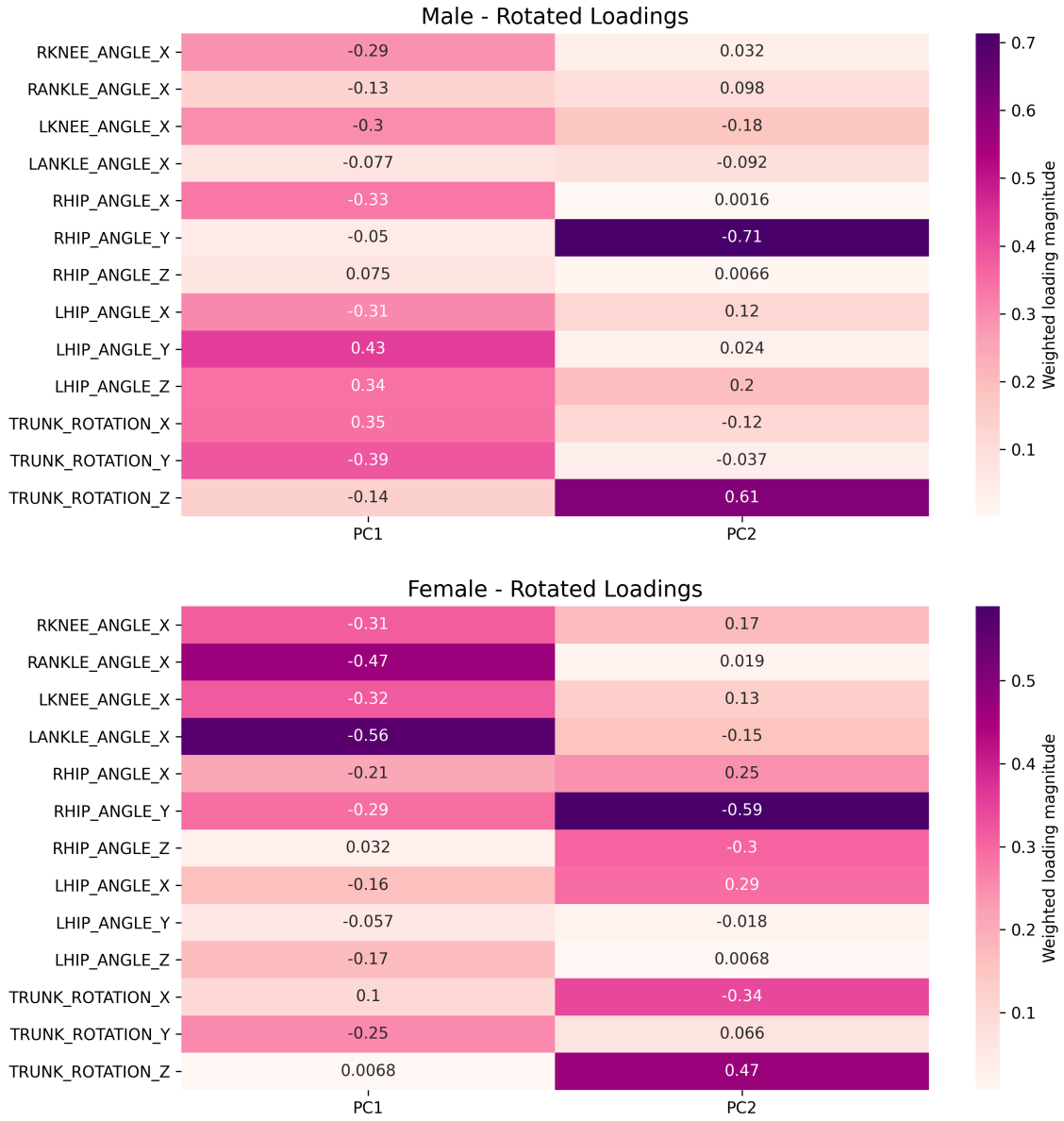

Figure 3.2: Heatmap representing the rotated loading scores of the two first PCs for male (up) and female (down). The color scale is based on the absolute values of the coefficients.

Same as for planning comparison, PCA was performed separately for males and females, with a Varimax rotation applied in each case to facilitate interpretation. The analysis is based on the heatmaps shown in Figure 3.2. Although the values themselves should not be directly compared, it is still possible to observe meaningful differences in joint contributions.

When comparing males and females, the rotated loading coefficients exhibit distinct patterns. For males, in PC1, the dominant variables are the three left hip angles, as well as trunk rotations in both the sagittal and frontal planes. Knee angles and the right hip angle in the sagittal plane also contribute, though to a slightly lesser extent. Among these, the knee angles, left and right hip angles in the sagittal plane and trunk rotation in the frontal plane have negative loadings, whereas the others are positive. This suggests that these sets of degrees of freedom move in opposite directions. In contrast, for females, the hip and trunk variables are less dominant in PC1. Instead, the movement is primarily driven by the ankle and knee angles. The right hip angle and trunk rotation in the frontal plane also contribute but less prominently. Interestingly, all loadings are negative in this case, indicating that all these degrees of freedom move in the same direction.

These observations are in line with the findings of Decker et al. [43], who reported gender differences in landing strategies. According to their study, females tend to rely more on the ankle musculature to attenuate impact, even in soft landings (defined by them as a maximum knee flexion angle greater than 90°). At initial ground contact, females typically show greater knee extension and ankle plantarflexion. This is consistent with these PCA results for females, where ankle and knee angles emerge as primary contributors to the variance in coordination patterns, indicating a coordinated movement strategy centered on these joints. However, this more erect landing posture may increase the risk of injury, particularly in cases of muscle fatigue or loss of postural control. Conversely, Decker et al. observed that males exhibit greater knee flexion and less ankle plantarflexion at ground contact. This posture enables more efficient energy transfer to the proximal muscles, such as the hip extensors. This is coherent with the presented results, where the hip, trunk, and knee angles explain most of the variance in males' coordination strategies. These insights highlight the importance of incorporating neuromuscular training programs that encourage greater knee flexion during landing. Such interventions are particularly relevant for female athletes, given their characteristic landing strategies. They may effectively help reduce the risk of lower limb injuries, including anterior cruciate ligament injuries.

Regarding PC2, the male pattern highlights two dominant variables : the right hip angle in the frontal plane (hip abduction/adduction) and trunk rotation in the transverse plane (axial rotation). These two loading coefficients have opposite signs, the hip coefficient is negative, while the trunk coefficient is positive, suggesting that these two joints move in opposite direction. For females, the pattern appears more distributed. While the same two variables remain prominent, additional contributions are observed from the right hip in the other two anatomical planes, the left hip in the sagittal plane, and trunk rotation in both the sagittal and transverse planes. The right hip angle and trunk axial rotation moving in opposite directions is also suggested for females. Among the other contributing joints, the left and right hip angles in the sagittal plane have positive loading coefficients, while the right hip angle in the transverse plane and trunk rotation in the sagittal plane have negative loading coefficients. Interestingly, although the hips are involved in the coordination pattern for females, their contribution appears in the second synergy rather than the first. This indicates that hip involvement is not part of the primary coordination strategy but

occurs later in the control sequence. Such a pattern suggests that females may rely on a different landing strategy, one that emphasizes distal control earlier in the movement and engages proximal segments, such as the hips, only in a secondary phase. This contrasts with the conclusions drawn for males, where the hip already contributes to the primary synergy, suggesting an earlier involvement of proximal control in their landing strategy. This remains consistent with the findings of Decker et al., who reported that female athletes tend to rely more heavily on distal joints, with delayed or reduced activation of the hip musculature during landing tasks.

3.2.3 Biomechanical variable analysis using SPM1D and descriptive methods

By observing the curves in Figure 3.3, and focusing on the female curve, the hypothesis that the main contributing joint synergies move in the same direction is confirmed. The dotted curves indicate that the knee and ankle joints on both sides move in the same direction, as an increase in ankle angle corresponds to an increase in knee angle. This pattern is also observed in males, but is less relevant since these joints do not form the primary synergies explaining movement variance in males. Nevertheless, some differences in joint angle values can be noted. Specifically, females exhibit a smaller knee flexion angle compared to males.

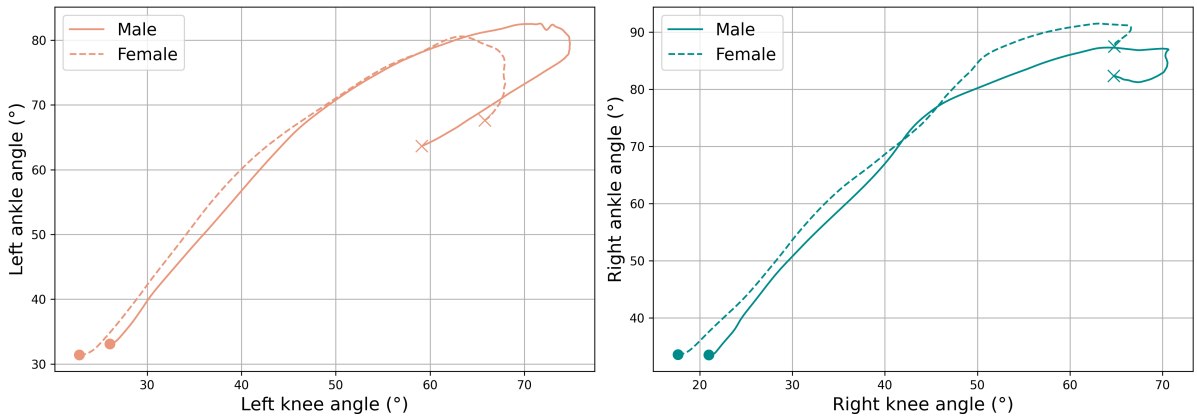

Figure 3.3: Angle-angle plots of knee and ankle joints in the sagittal plane for male and female. The landing phase starts at the dot and ends at the cross.

To better understand the differences between males and females, it is useful to deepen the analysis by examining the GRFs. From Figure 3.4, several observations and conclusions can be made. First, note that the GRF curves have been normalized. Each GRF was normalized by the individual body weight of each subject. Then, mean curves and standard deviations were computed. Normalization is essential in this case because males and females represent different subject groups with different body weights. In contrast, when comparing planned and unplanned situations, the same set of subjects was used. Therefore, normalization would not have affected the shape of the curves in that context. This explains why normalization is applied here and not in the previous comparison.

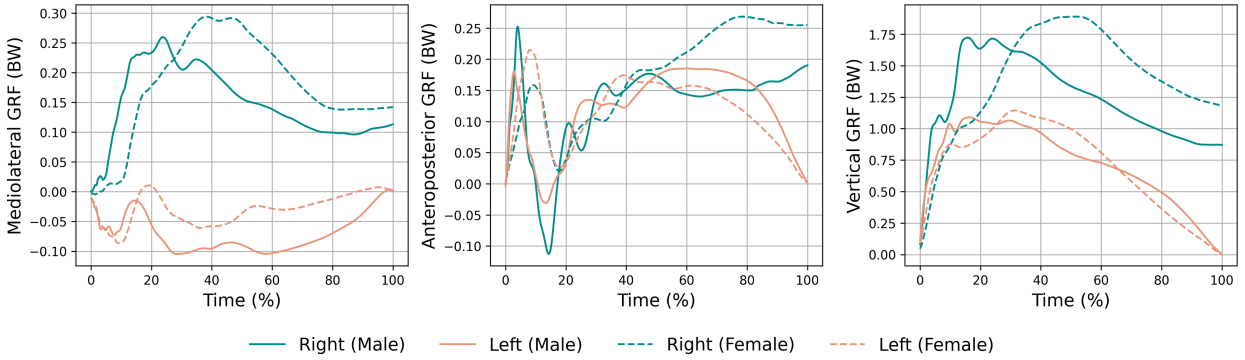

Figure 3.4: Ground reaction forces along the three spatial directions as a function of normalized time comparing male and female.

First, the vertical GRFs are quite similar in terms of amplitude between males and females. Although vertical GRFs are similar in amplitude between sexes, it is important to highlight that joint loading, particularly knee abduction moments, is not solely dictated by force magnitude. As previously shown in sidestep cutting study from Kristianslund et al. [44], alignment of the lower limb affects the moment arm of the GRF, which in turn significantly influences joint loading. Even subtle differences in movement timing or segment orientation may alter this alignment and increase joint moments despite similar GRF magnitudes. These considerations highlight the importance of segmental coordination in modulating joint loading. Inadequate or less effective coordination may result in non optimal lower limb alignment at ground contact, thereby altering the GRF lever arm and increasing joint moments despite similar external force magnitudes.

Moreover, in terms of timing, the peak of vertical GRF occurs later for females and appears smoother. This delay could stem from a slower neuromuscular adaptation, meaning the muscles take longer to react to impact. Notably, for females, the heatmap highlighted the ankle as a standout joint in coordination, which was not the case for males. Referring to Figure 3.5 and 3.6, the difference in ankle and knee angles between males and females appears minimal. At initial ground contact, the difference is not significant, thus rejecting an hypothesis about joint angle differences. However, the neuromuscular hypothesis remains plausible. In Figures 3.4, 3.5 and 3.6, the slope of the curves depicting the temporal evolution of the ankle and knee angles and GRFs is steeper for males than for females. This indicates a slower rate of increase in both joint angles and ground reaction forces in females. Specifically, in the ankle and knee angle plots, dorsiflexion and knee flexion occur more gradually in females. Similarly, the vertical GRF reaches its maximum slightly later in females, suggesting a delayed peak force. These temporal differences may reflect variations in movement strategies or neuromuscular control between sexes.

Furthermore, the difference in ankle angle between males and females is statistically significant from approximately 7% to 20% of the landing phase, an early stage in the movement as can be seen in Figure 3.5. This means that, even though the angle at initial ground contact is roughly the same, differences emerge shortly afterward and then become non-significant later in the phase. This supports the idea that the ankle joint moves at different speeds in the two groups, possibly due to slower muscular activation in females. A similar pattern, following the previous reasoning, may be observed for the knee joint in Figure 3.6. However, the significant differences are less pronounced, suggesting that the ankle joint primarily contributes to the observed effect. This conclusion is also supported by a study by Hunter et al. [45], which states that muscle contraction is faster in males. They have a greater proportion of type II muscle fibers, which exhibit a higher shortening velocity compared to type I fibers. In contrast, females tend to have a higher proportion of type I fibers, which contract more slowly but are more resistant to fatigue. As males have a larger cross-sectional area occupied by these fast-twitch fibers, this results in a faster overall muscle contraction. Conversely, female muscles are more fatigue-resistant but exhibit slower relaxation and contraction speeds. Note that, as the data were time-normalized, these timing differences may partially reflect variations in the duration of the landing phase between sexes. Without access to absolute time values, it remains uncertain whether the peaks are truly delayed in real time or shifted due to longer movement durations.

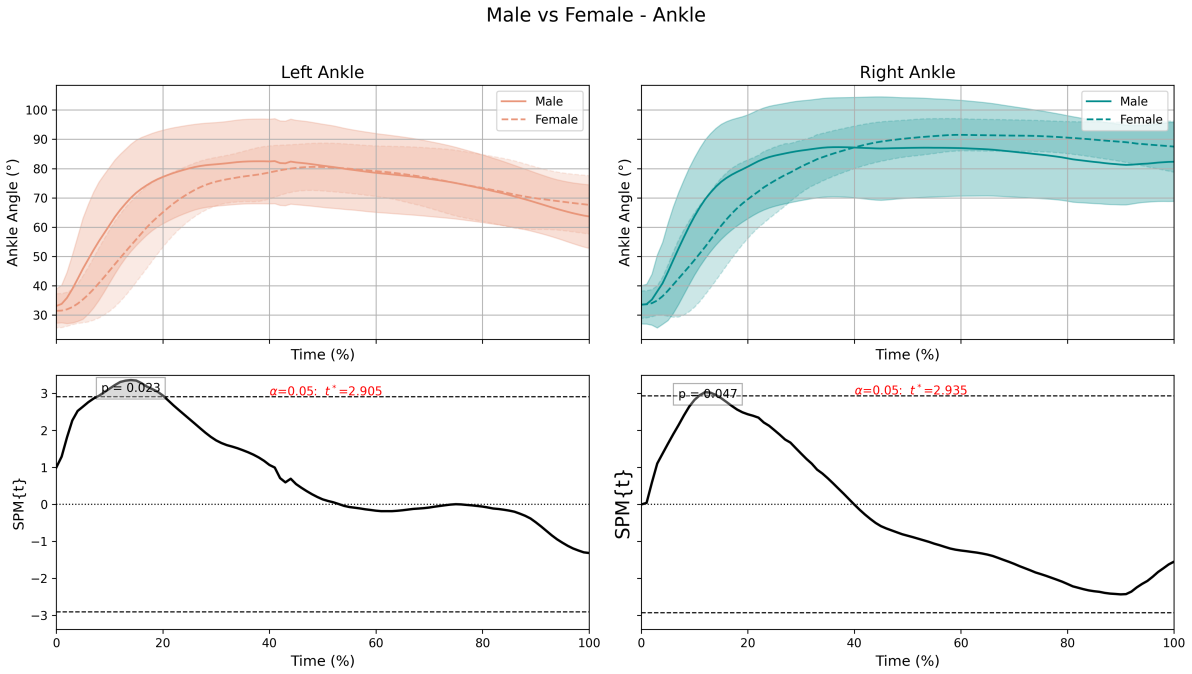

Figure 3.5: Mean temporal evolution of the left and right ankle angles (top row). SPM1D t-test results comparing males and females for ankle angles (bottom row).

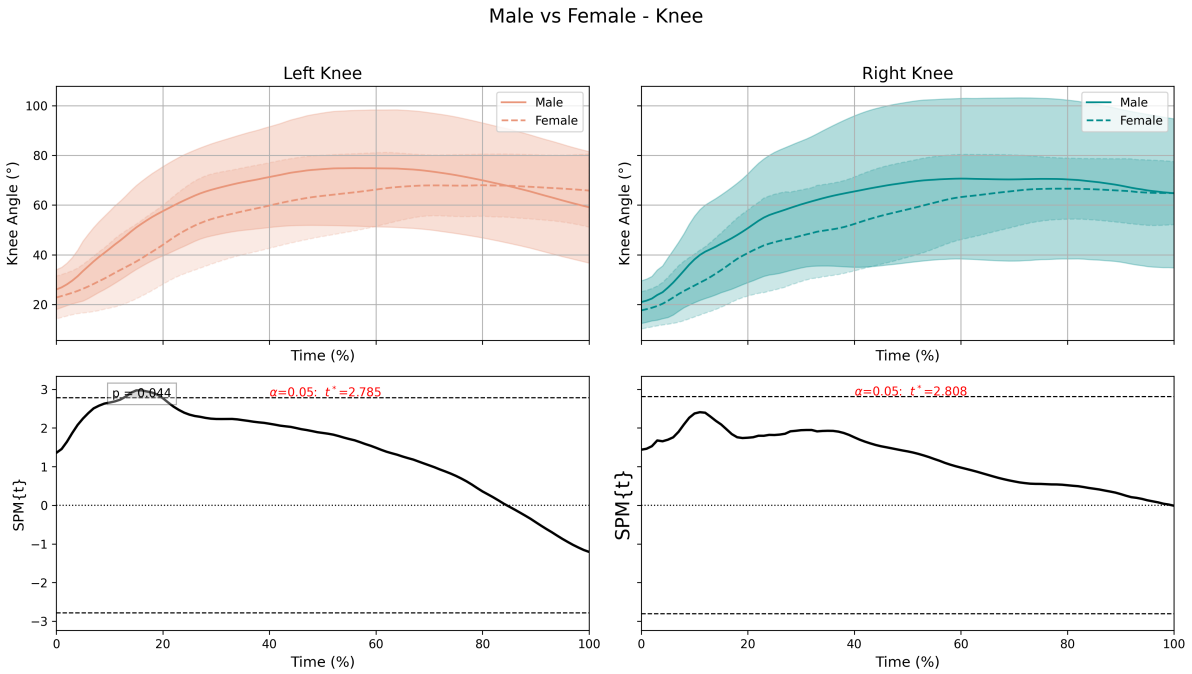

Figure 3.6: Mean temporal evolution of the left and right knee angles (top row). SPM1D t-test results comparing males and females for knee angles (bottom row).

Coming back to the GRF amplitude, male and female GRFs were compared statistically using SPM1D. On the left foot, as shown in Figure 3.7, there are no significant differences in any of the three GRF components. On the right foot, however, Figure 3.8 highlights some differences. These differences are generally small, as the statistical threshold is barely exceeded, except for one case. For the vertical GRF, a more noticeable difference is observed around 60% of the movement cycle, where the threshold is exceeded over a slightly longer duration. This difference occurs when the male GRF has already started to decrease. At the same time, the female GRF peak appears wider and more delayed, resulting in a higher value at that point. This observation is consistent with the previously discussed differences in muscle fiber properties between males and females. Specifically, it aligns with the fact that female muscles tend to exhibit slower relaxation speeds. Nevertheless, as already mentioned, the lack of access to absolute time values necessitates caution in interpreting the observed timing differences.

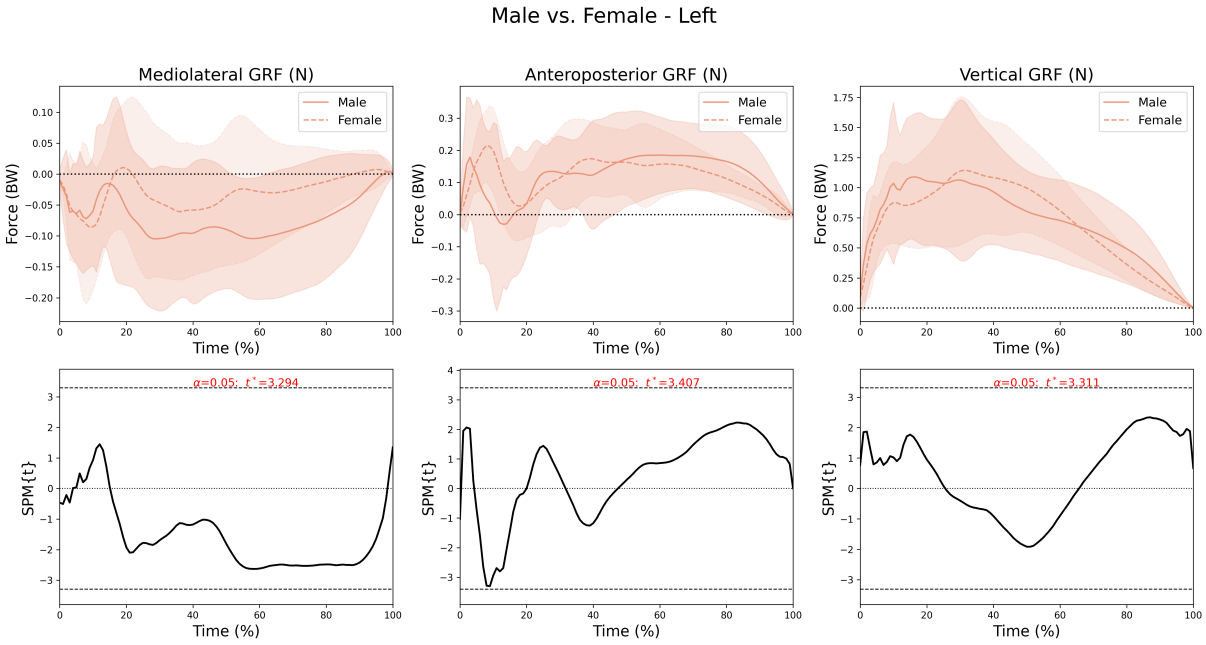

Figure 3.7: Mean GRF in three spatial directions with standard deviation (top row). SPM1D t-test results comparing male and female for the left foot (bottom row).

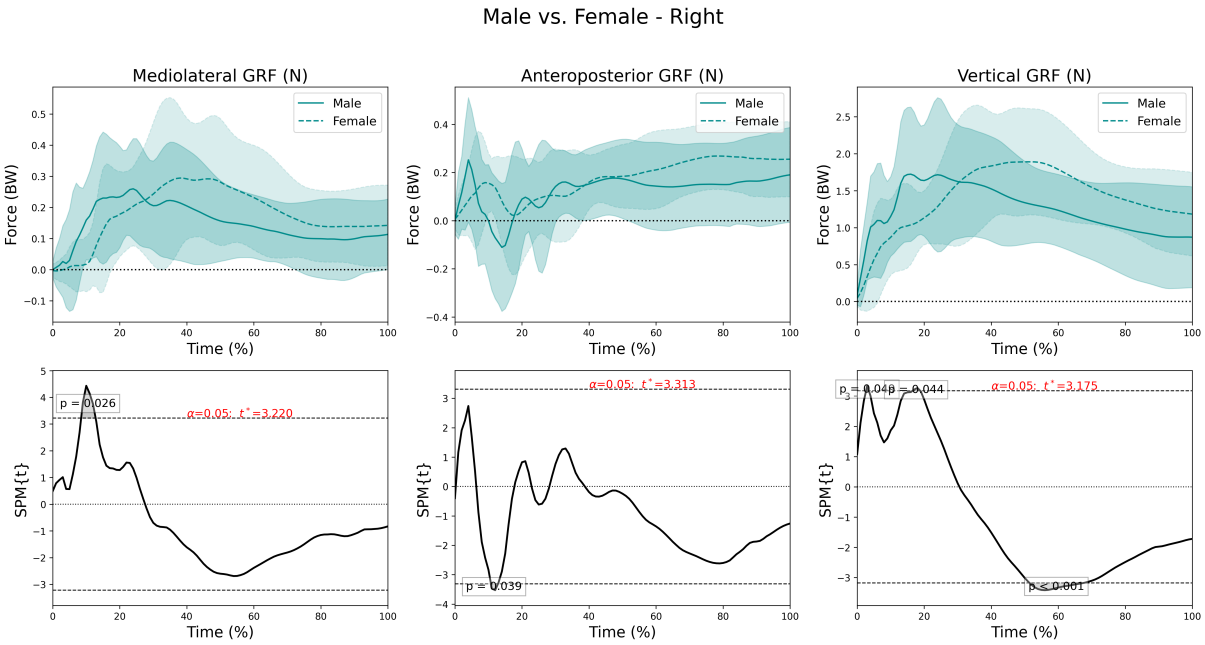

Figure 3.8: Mean GRF in three spatial directions with standard deviation (top row). SPM1D t-test results comparing male and female for the right foot (bottom row).

Afterwards, left and right feet were compared separately for males and females. This comparison is based on Figures 3.9 and 3.10. As previously observed when comparing left and right feet in the planned and unplanned conditions, the mediolateral GRF shows a significant difference over almost the entire movement, as the forces act in opposite directions on each foot. Regarding the vertical GRF, while differences in the planned vs. unplanned comparison began early in the movement (around 20%), this is not the case when comparing left and right feet in males and females. For females, significant differences between the left and right foot appear later, around 40% of the movement, and persist until the end. In contrast, for males, the differences occur in two phases: the first from approximately 15% to 70%, and the second from around 85% to the end. However, when the curve drops below the significance threshold, it remains relatively close to it. Moreover, the level of significance is notably higher for females, while it remains lower for males. This could suggest that females transfer their weight to the right leg later in preparation for the opening step. They initially land on both feet in a relatively symmetrical manner, followed by a marked difference. In contrast, although a weight transfer is also evident in males, it appears to be less pronounced or more variable. The weight shift occurs earlier but is less distinct.

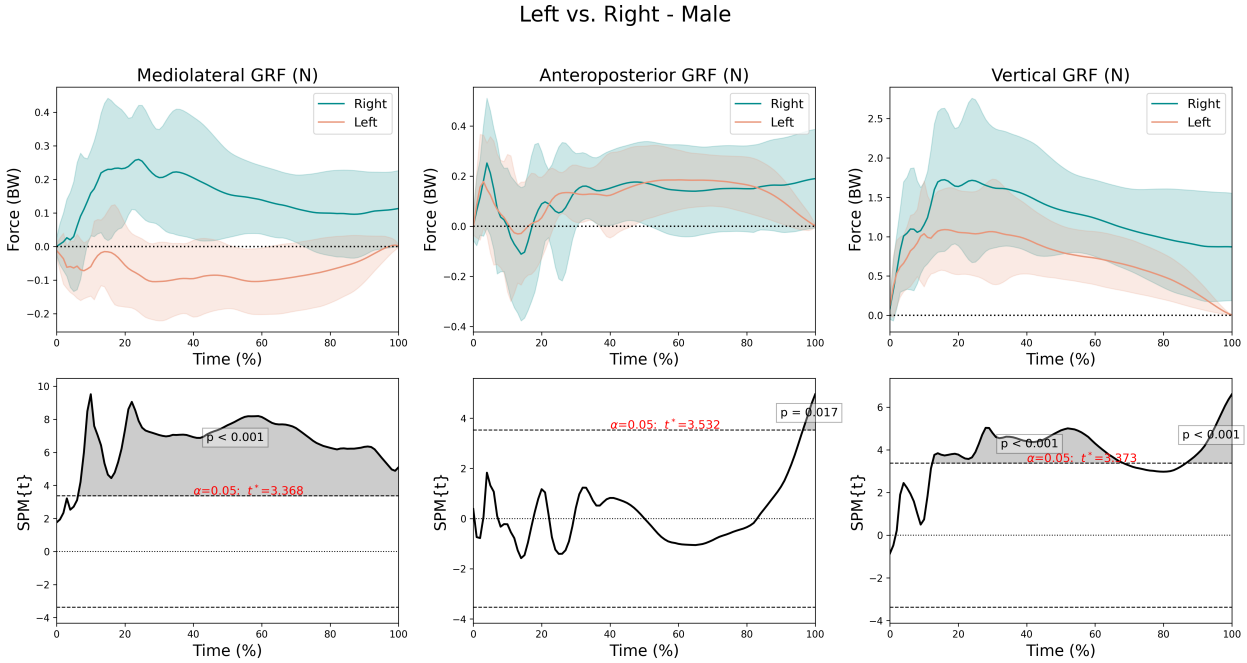

Figure 3.9: Mean GRF in three spatial directions with standard deviation (top row). SPM1D t-test results comparing left and right feet for males (bottom row).

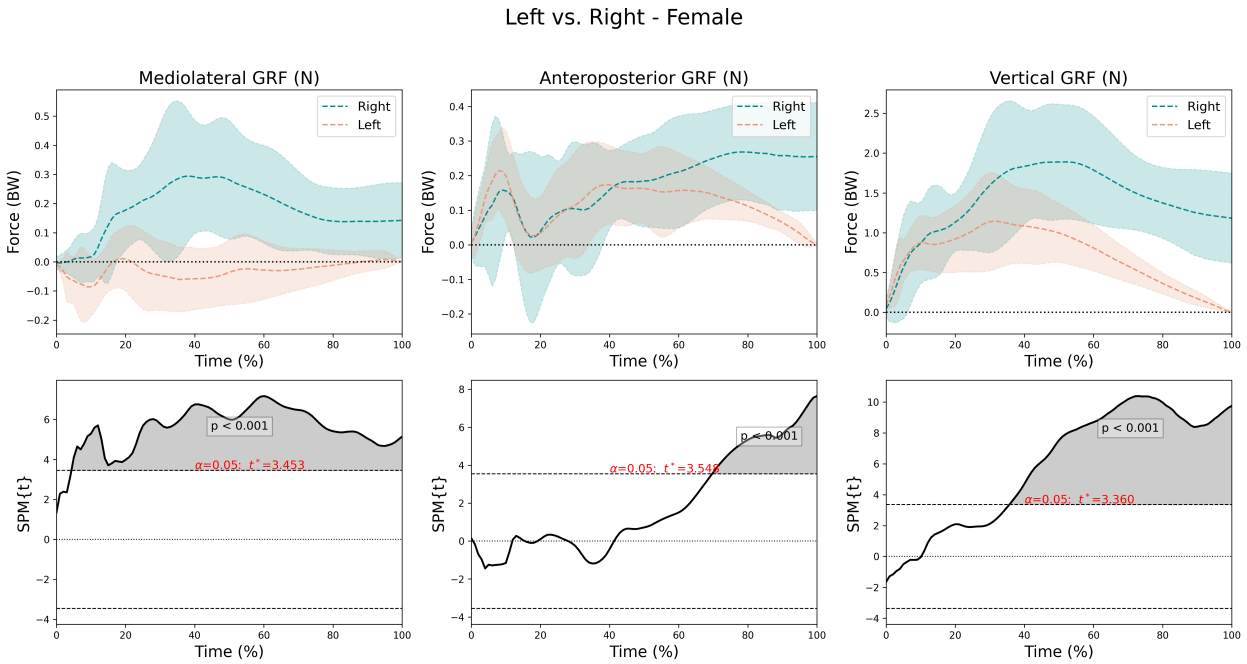

Figure 3.10: Mean GRF in three spatial directions with standard deviation (top row). SPM1D t-test results comparing left and right feet for females (bottom row).

After completing the PC1 analysis, a more detailed examination of PC2 also yields interesting insights. For both males and females, the right hip angle in the frontal plane and trunk axial rotation emerge as being involved in a common coordination pattern. As highlighted in the heatmap analysis section, these two joints appear to move in opposite directions, based on the opposite signs of their loading coefficients. This observation is confirmed in Figure 3.11, particularly during the second phase of the movement. Initially, both the right hip angle and trunk rotation angle increase. However, at around 50% of the movement, while the trunk rotation continues to increase, the right hip angle begins to decrease. This pattern is also evident in Figure 3.12, which illustrates the temporal evolution of each joint angle. This behavior is consistent across both males and females. No significant gender differences were observed for either the right hip angle or the trunk rotation angle.

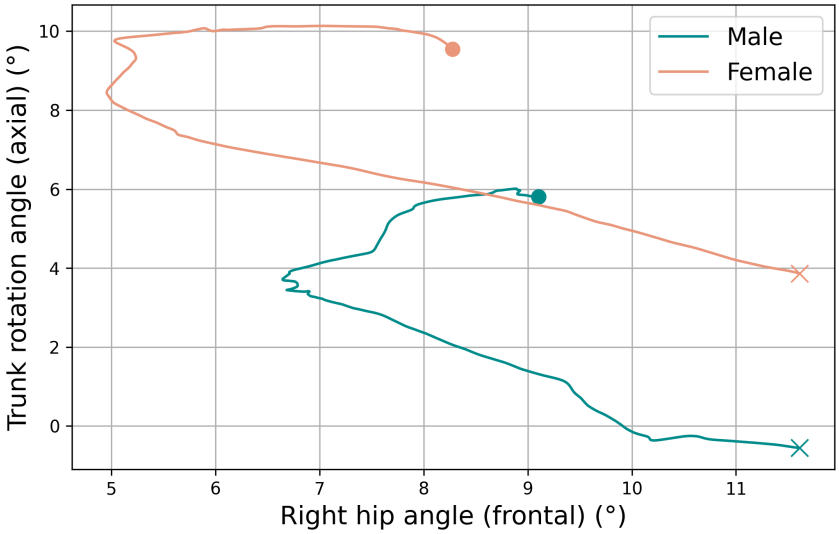

Figure 3.11: Angle-angle plot of right hip in the frontal plane and trunk axial rotation comparing male and female. The landing starts at the dot and ends at the cross.

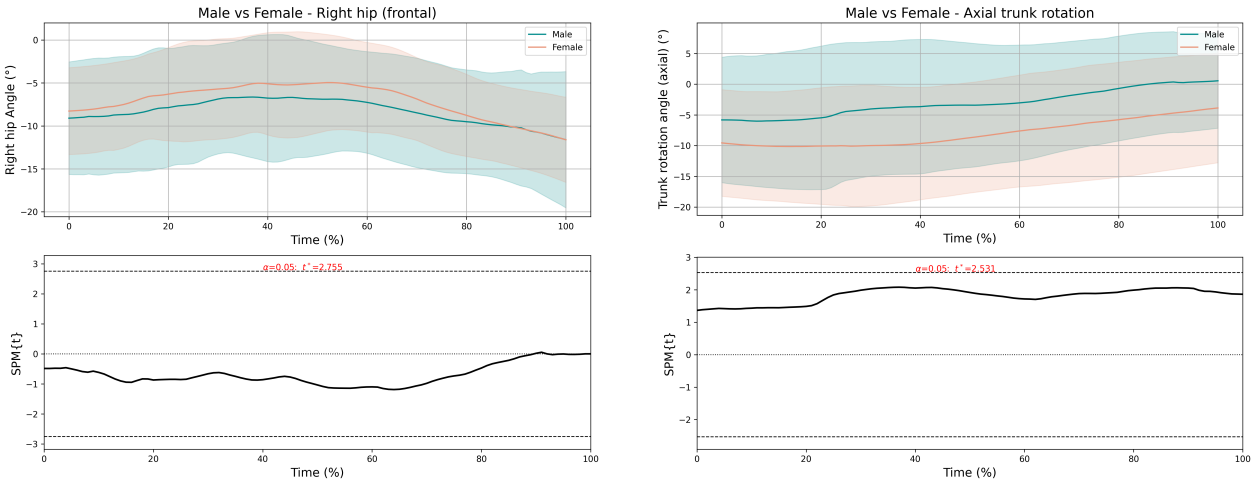

Figure 3.12: Mean temporal evolution of the right hip (frontal) and trunk rotation (axial) angles (top row). SPM1D t-test results comparing males and females for these angles (bottom row).

3.2.4 Comparison with previous studies

In the previous study from Decker et al. [43], the authors focused on identifying gender differences in lower extremity kinematics and kinetics during landing. Their protocol, stepping off a 60 cm box, was similar to the one used in the present study. In this, vertical GRF displayed very similar patterns, without any specific conclusions regarding magnitude or timing differences. In the present study, although the amplitude does not highlight significant gender differences, the force curves do not perfectly overlap. As previously explained, a delayed response is observed in females. Therefore, unlike the findings in Decker et al., this study reveals timing differences between genders.

In another study by Ford et al. [46], the authors analyzed joint stiffness across genders during maturation and in post-pubertal athletes. The protocol involved participants dropping off a 31-cm box and immediately performing a maximal vertical jump. They drew several conclusions about gender differences in motor control that are relevant to the present study. According to their findings, post-pubertal males and females exhibit different strategies. Females tend to adopt a knee-dominant strategy, relying more on the knee joint for force absorption, to the detriment of the hip and ankle joints. In contrast, males distribute the load more evenly, with greater involvement of the hip and ankle joints, demonstrated by increased hip flexion at impact and higher joint moments at these joints. This more balanced strategy in males was also associated with greater active stiffness at the hip and ankle, indicating a more effective neuromuscular strategy for joint stabilization during dynamic tasks.

Some of these findings align with those of the current study. Specifically, the observation that males tend to adopt a hip-dominant landing strategy is consistent with the present results, as shown in the heatmap : in PC1, the hip joint contributed most prominently to the movement. However, unlike Ford et al., a strong contribution from the ankle joint in males

was not observed. Regarding females, the knee-dominant landing strategy reported by Ford et al. is partially supported by the present data. Indeed, the heatmap indicated that the knee joints were major contributors in PC1. Nonetheless, the ankle joints also contributed significantly, which somewhat differs from the knee-dominant pattern described by Ford et al. Moreover, in terms of hip angle values, no significant differences were found between males and females according to the SPM1D analysis, as shown in Figure 3.13. However, the standard deviation is notably greater for males, suggesting that inter-trial and/or inter-individual variability is higher in this group. This implies that males do not exhibit a homogeneous landing strategy, whereas females tend to display more consistency in their landing patterns. This higher standard deviation observed in males is also apparent in previous graphs comparing males and females, where the male curves often show greater variability.

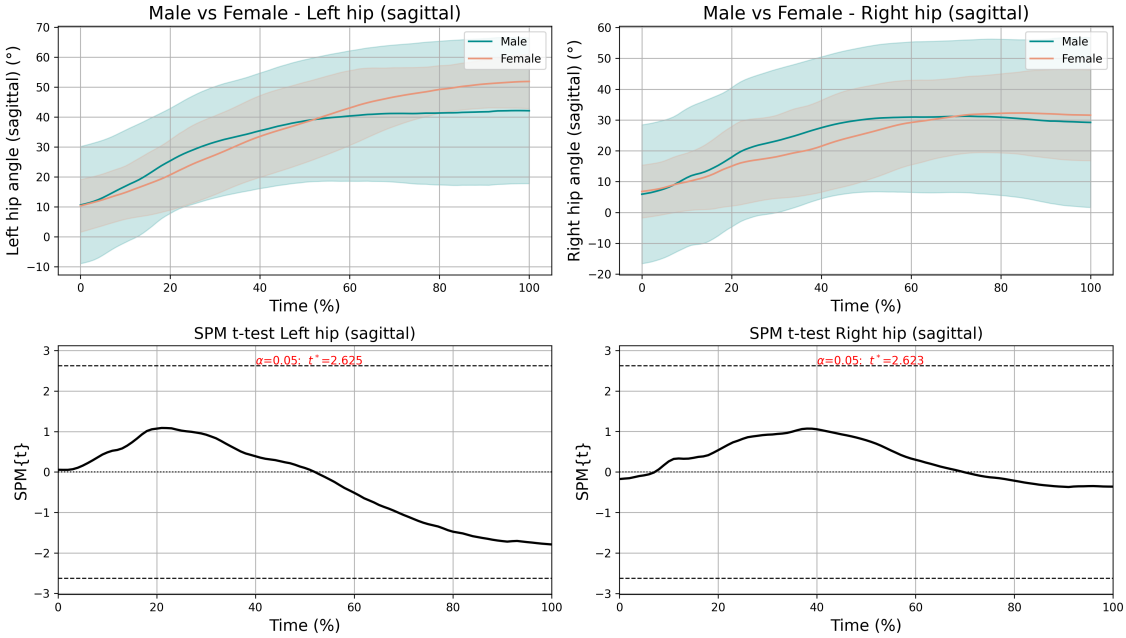

Figure 3.13: Mean temporal evolution of the left and right hip (sagittal) angles (top row). SPM1D t-test results comparing males and females for these angles (bottom row).

3.2.5 Gender difference conclusion

As a conclusion for the analysis of gender differences in joint coordination, it appears that, for females, the majority of the movement is governed by more distal joints, i.e., the ankles and knees, which tend to move in the same direction. Secondly, the hip and trunk also contribute to the movement, but to a lesser extent. In contrast, males exhibit a more distributed coordination pattern across multiple joints. Proximal joints such as the hip and trunk are more heavily involved, along with the knees. Additionally, the secondary joints contributing to coordination in males seem to operate in a more direction-specific manner, whereas in females, joint involvement appears more uniform across joints and anatomical planes.

Interestingly, although the PCA and heatmap analyses clearly highlight these coordination differences, they are not always distinctly reflected in the angle-angle plots or individual joint time series. Differences were sometimes observed, but only during specific phases of landing. In other cases, no significant differences were found at all. This apparent discrepancy highlights the fact that coordination is not solely defined by the isolated movement of individual joints, but rather by the relationship between them. In this regard, multivariate analyses such as PCA are particularly valuable, as they reveal subtle inter-joint interactions and underlying motor strategies that may remain hidden in traditional joint-by-joint evaluations. Thus, the PCA results offer a complementary perspective that deepens our understanding of global coordination mechanisms. Nevertheless, joint-by-joint analyses still provide essential information such as asymmetries or specific joint behavior that complement the multivariate findings. Moreover, greater inter-individual variability was observed in males, suggesting that male participants employed a wider range of landing strategies. In contrast, females displayed more consistent joint behavior, indicating a more homogeneous motor pattern across individuals.

Finally, the GRF analysis provides physiological insight that complements the kinematic findings. Although GRF amplitudes were similar after normalization, females showed delayed and smoother force peaks, suggesting a slower neuromuscular response. This aligns with observed differences in ankle motion and is consistent with known gender-based differences in muscle fiber composition. Additionally, females exhibited more consistent weight transfer patterns, possibly indicating a more anticipatory or stabilized motor strategy compared to the more segmented response observed in males. These findings may have practical implications for neuromuscular training programs, which could be tailored to address sex-specific landing patterns and reduce the risk of lower limb injuries.

Chapter 4

Limitations

This fourth chapter provides an in-depth analysis of the limitations encountered during this work, while also treating them as opportunities for future research enhancements.

4.1 Limitations related to the experimental protocol

One key limitation lies in the test setup. Because separate force plates were used to measure the ground reaction forces of each foot, participants had to place one full foot on each plate without overlap. This constraint forced them to land facing the wall, with their feet roughly parallel, unlike a typical volleyball landing. Usually, players anticipate the next action, begin trunk rotation and often touch down with one foot ahead of the other. Additionally, the dimensions of the force plates offered very little margin for error. In the anterior-posterior direction, each force plate measured only 40 cm, meaning the foot could easily step off the plate. Consequently, athletes had to modify their habitual movement pattern, likely over-thinking each landing and producing less natural motions. These are elements that could introduce errors into the data.

Another limitation of the laboratory setup is that only right-side blocks were analyzed. With just two force-plates available, both were installed on the right, so GRFs from left-side blocks could not be recorded. In addition, the net was set slightly off-center. Thus, movements on the right remained fully within the cameras' field of view, but actions on the left drifted outside the optimal capture zone, causing frequent marker loss and making reliable kinematic data impossible on that side. However, due to their role and typical position on the court, some players are not familiar to blocking on their right side. This constraint is not problematic for middle blockers, who routinely block on both sides. In contrast, left-side hitters typically block on the left. So, asking them to block on the right may have felt unfamiliar and thus less natural, potentially altering their movement patterns. While this represents a clear limitation, it also presents an opportunity. Future work could compare joint coordination during blocks executed on a player's habitual versus non-habitual side to explore side-specific adaptations.

4.2 Others

Another limitation, related more to the sample size, concerns the number of participants tested. As detailed in Section 2.1.2, the power analysis indicated that 40 participants were required. However, the actual sample was limited to 20 subjects, which may lead to findings occurring by chance due to the lack of representativeness of the population. Therefore, it would be beneficial to extend this study to a larger sample to either confirm or refute the results and conclusions presented here. Nonetheless, this study serves as a valuable preliminary investigation that highlights some initial trends.

Finally, the uncontrolled inter-individual variability between the participants may also be a limitation. Although all subjects performed the same experimental tasks, individual characteristics such as dominant side, volleyball experience, habitual motor strategies, playing position on the court or even responsiveness to unexpected stimuli, may have influenced their movement coordination. For example, a middle blocker, frequently involved in blocking actions requiring side-decision making, may exhibit different coordination strategies than a player occupying the outside hitter or opposite positions, where the frequency and type of blocks may differ. These role-specific differences in blocking can lead to distinct motor patterns even under similar experimental conditions. This variability introduces heterogeneity within the experimental groups, which could obscure the effects specifically associated with the planned versus unplanned conditions. While such diversity reflects real-world game situations, it also limits the ability to generalize the findings. Future studies may benefit from controlling for or stratifying participants based on factors such as laterality, playing position and level of experience.

Chapter 5

Conclusion

Understanding joint coordination is fundamental in sports requiring rapid transitions and high-intensity movements. In volleyball, especially during blocking actions, the landing phase plays a crucial role in both performance and injury prevention. This research aimed to investigate inter-joint coordination during landing after a block, with particular emphasis on the effects of unplanned versus planned conditions and gender-related differences.

To achieve this, an experimental protocol was implemented involving male and female volleyball players performing block landings in a motion analysis laboratory. A combination of motion capture system, force plate measurements, and electromyography was used to collect data. To extract meaningful information about coordination patterns, both classical biomechanical analyses and Principal Component Analysis (PCA) were applied.

A literature review highlighted the variety of existing methods to assess inter-joint coordination, each offering different perspectives. Among these, PCA was selected for its ability to identify global coordination patterns by reducing dimensionality while preserving essential movement information. This multivariate approach proved particularly suitable for revealing subtle inter-joint relationships often overlooked in joint-by-joint analyses.

The PCA results showed that coordination differences between genders were more pronounced than those observed between planned and unplanned conditions. In both planned and unplanned landings, two principal components were sufficient to explain most of the variance, suggesting a similar overall motor control strategy regardless of anticipation. Distal joints, particularly the ankle and knee, played a leading role in energy absorption, with slightly more proximal involvement, hip and trunk, observed in planned situations. This may reflect a more balanced segmental control when anticipation is possible. The lack of marked differences between planned and unplanned conditions may be partly explained by the experimental setup. In the unplanned situation, the direction of the block was indicated as a trigger for trial onset. This potentially allowed participants to preprogram their motor strategy during the first part of the movement, i.e. three-step jump, thereby reducing the unpredictability intended in the unplanned condition. Moreover, the presence of force plates

and the constraint to land on them likely induced an internal focus during landing in both planned and unplanned situations. This could have restricted natural movement patterns and limited the ecological validity of the task.

In contrast, clear distinctions in coordination strategies were observed between males and females. Female participants demonstrated movement strategies primarily governed by distal joints, with more uniform involvement across joints and anatomical planes. Males, on the other hand, exhibited more distributed and direction-specific coordination patterns, including greater reliance on proximal joints. Additionally, males showed higher inter-individual variability, suggesting a broader range of motor strategies, whereas females displayed more consistent movement patterns. These findings were further supported by the ground reaction force (GRF) analysis, which revealed sex-specific differences in neuromuscular responses. Females exhibited a slower rate of increase of joint angles, possibly indicating slower but more controlled landing strategies, consistent with known muscle composition differences. Moreover, their weight transfer appeared more stable and anticipatory than that of males, whose landing behavior was more segmented.

In addition, asymmetries between the lead and trail leg were observed, particularly in the timing and amplitude of joint contributions during landing. These findings, although not the main focus, highlight the potential importance of lateral dominance in joint coordination and injury risk, and warrant further investigation.

Together, these results demonstrate the complexity and adaptability of joint coordination, particularly in response to uncertainty and across genders. They also underscore the added value of combining multivariate analyses like PCA with classical biomechanical methods to obtain a more comprehensive understanding of motor control.

Limitations of the study include the timing of the directional cue and the constraints imposed by the laboratory setting, which may have reduced the ecological validity of the unplanned condition. Furthermore, the sample may have included considerable variability in terms of player experience, court position or dominant side, which could have influenced coordination patterns. Future studies should aim to introduce more unpredictable scenarios and consider creating more homogeneous subject clusters to enhance the comparability of results.

In conclusion, this research contributes to a better understanding of landing coordination in volleyball, offering insights that may inform injury prevention strategies and the development of sex-specific training protocols. Future studies are nonetheless required to confirm these findings and to support the integration of biomechanical knowledge into applied sports training and rehabilitation.

Bibliography

[1] W. K. Young et al. “Epidemiology of Common Injuries in the Volleyball Athlete”. In: *Current reviews in musculoskeletal medicine* Vol.16 (6) (June 2023), p.229–234.

[2] D. Pereira et al. “Fatigue-induced modifications to trunk and lower-limb coordination mode during drop vertical jump and sidestep cutting tasks in female handball athletes”. In: *Gait posture* Vol.117 (Mar. 2025), p.45–53.

[3] C. Chinnasee et al. “A Biomechanical Comparison of Single-Leg Landing and Unplanned Sidestepping”. In: *International journal of sports medicine* Vol.39 (8) (July 2018), p.636–645.

[4] D. Gates J. Cowley. “Inter-joint coordination changes during and after muscle fatigue”. In: *Elsevier* Vol.56 (Pt B) (Dec. 2017), p. 109–118.

[5] P. Fuchs et al. “Effects of Differential Jump Training on Balance Performance in Female Volleyball Players”. In: *Applied sciences* Vol.10 (17) (Sept. 2020), p.5921.

[6] F. Daniel Tik-Pui et al. “Effect of anticipation on knee kinematics during a stop-jump task”. In: *Gait posture* Vol.39 (1) (Jan. 2014), p.75–79.

[7] J. Connor et al. “Effect of Different Evasion Maneuvres on Anticipation and Visual Behavior in Elite Rugby League Players”. In: *Motor Control* Vol. 22 (Jan. 2017), p. 1–17.

[8] S. Han et al. “Effects of anticipation on joint kinematics during inversion perturbation in individuals with chronic ankle instability”. In: *Scandinavian journal of medicine science in sports* Vol.33 (7) (July 2023), p.1116–1124.

[9] C. Shirota et al. “On the assessment of coordination between upper extremities: towards a common language between rehabilitation engineers, clinicians and neuroscientists”. In: *Journal of neuroengineering and rehabilitation* Vol.13 (1) (Sept. 2016), p.80–80, Article 80.

[10] K. Young Kwan et al. “Inter-joint coordination in producing kicking velocity of taekwondo kicks”. In: *Journal of sports science medicine* Vol.10 (1) (Mar. 2011), p. 31–38.

[11] D. S. Irawan et al. “Concurrent Validity and Reliability of Two-dimensional Frontal Plane Knee Measurements during Multi-directional Cutting Maneuvers”. In: *International journal of sports physical therapy* Vol.17 (2) (2022), p.148–155.

[12] M.-T. Puth et al. “Effective use of Pearson’s product-moment correlation coefficient”. In: *Animal behaviour* Vol.93 (July 2014), p.183–189.

[13] D. S. Moore. *The basic practice of statistics (6th ed.)* New York, NY : W. H. Freeman, 1995.

[14] O. Dubois et al. "A guide to inter-joint coordination characterization for discrete movements: a comparative study". In: *Journal of neuroengineering and rehabilitation* Vol.20 (1) (Sept. 2023), p.1–132, Article 132.

[15] S. Yoon S. Park. "Quantifying Coordination and Variability in the Lower Extremities after Anterior Cruciate Ligament Reconstruction". In: *Sensors* Vol.21 (2) (Jan. 2021), p.652.

[16] Q. Huang et al. "Intra-limb joint coordination measures of upper limb and hand movements: A systematic review". In: *Gait posture* Vol.108 (Feb. 2024), p.289–300.

[17] P. Lamb and M. Stöckl. "On the use of continuous relative phase: Review of current approaches and outline for a new standard". In: *Clinical biomechanics (Bristol)* Vol.29 (5) (May 2014), p.484–493.

[18] A. Sidiropoulos et al. "Implementation of relative phase analysis to evaluate continuous interlimb coordination and stability in individuals with lower limb loss: Design and protocol for a retrospective analysis". In: *BMJ open* Vol.13 (11) (Nov. 2023), p.e072265–e072265.

[19] B. Peters et al. "Limitation in the use and interpretation of continuous relative phase". In: *Journal of biomechanics* Vol.36 (2) (Feb. 2003), p.271–274.

[20] A.J. Harrison et al. "Functional data analysis of joint coordination in the development of vertical jump performance". In: *Sports biomechanics* Vol.6 (2) (May 2007), p.199–214.

[21] P. Jae Hyeon et al. "Effects of knee osteoarthritis severity on inter-joint coordination and gait variability as measured by hip-knee cyclograms". In: *Scientific reports* Vol.11 (1) (Jan. 2021), p. 1789–1789, article 1789.

[22] R. Di Giminiani et al. "Angle-Angle Diagrams in the Assessment of Locomotion in persons with Multiple Sclerosis: A Preliminary Study". In: *Applied sciences* Vol.12 (14) (July 2022), p.7223.

[23] E. Cushion et al. "Principal Component Analysis Reveals the Proximal to Distal Pattern in Vertical Jumping Is Governed by Two Functional Degrees of Freedom". In: *Frontiers in bioengineering and biotechnology* Vol.7 (Aug. 2019), p.193–193.

[24] J. Keogh et al. "Longitudinal Monitoring of Biomechanical and Psychological State in Collegiate Female Basketball Athletes Using Principal Component Analysis". In: *Translational sports medicine* Vol.2024 (2024), p.1–14.

[25] L. Ting and S. Chvatal. "Motor Control : Theories, Experiments, and Applications". In: ed. by F. Danion and Mark L. Latash. Oxford University Press, 2010. Chap. Decomposing Muscle Activity in Motor Tasks : Methods and Interpretation.

[26] Qualisys. *Qualisys – Motion Capture Systems and Biomechanics Solutions*. URL: https://www.qualisys.com/ (visited on 05/21/2025).

[27] Kistler Group. *3D force plates*. URL: https://www.kistler.com/INT/en/cp/3d-force-plates-with-digital-output-9667aa/P0001274 (visited on 05/21/2025).

[28] Delsys. *Trigno Avanti Sensor*. URL: https://delsys.com/product/trigno-avanti/ (visited on 05/21/2025).

[29] C. Schwartz. "Human Movement Analysis lecture, part 2 : Kinematics". 2024.
[30] Qualisys. *Processing your data - Fill types*. URL: https://docs.qualisys.com/getting-started/content/getting_started/processing_your_data/processing_your_data.htm (visited on 04/30/2025).
[31] G. Bi et al. "Impact of different landing heights on the contact force in the medial tibiofemoral compartment and the surrounding muscle force characteristics in drop jumps". In: *PloS one* Vol.19 (7) (July 2024), p.e0307538.
[32] J. Markström A. Strong. "Adding secondary cognitive tasks to drop vertical jumps alters the landing mechanics of athletes with anterior cruciate ligament reconstruction". In: *Journal of biomechanics* Vol.180 (Feb. 2025), p.112496, Article 112496.
[33] Y. Shimokochi F. Henderson. "Inertial One-Leg Squat Training and Drop Jump Biomechanics in Athletes With Anterior Cruciate Ligament Reconstruction After Return to Sport". In: *Journal of strength and conditioning research* Vol.39 (2) (Feb. 2025), p.156–164.
[34] J. Pedley et al. "Analyzing Drop Jump Ground Reaction Forces in Microsoft Excel". In: *Strength Conditioning Journal* Vol 45 (6) (Dec. 2023), p 683–697.
[35] S. Ohji et al. "Relationship Between Single-Leg Vertical Jump and Drop Jump Performance, and Return to Sports After Primary Anterior Cruciate Ligament Reconstruction Using Hamstring Graft". In: *International journal of sports physical therapy* Vol.19 (10) (Jan. 2024), p.1204–1215.
[36] T. Pataky. "One-dimensional statistical parametric mapping in Python". In: *Computer methods in biomechanics and biomedical engineering* Vol.15 (3) (Mar. 2012), p.295–301.
[37] T. Pataky. *SPM1D Python documentation*. URL: https://spm1d.org/Documentation.html (visited on 05/23/2025).
[38] S. Zhang et al. "Contributions of lower extremity joints to energy dissipation during landings". In: *Medicine and science in sports and exercise* Vol.32 (4) (Apr. 2000), p.812–819.
[39] E. Todorov and M. I. Jordan. "Optimal feedback control as a theory of motor coordination". In: *Nature neuroscience* Vol.5 (11) (Nov. 2002), p.1226–1235.
[40] M Bishop et al. "Do people with Parkinson's disease change strategy during unplanned gait termination?" In: *Neuroscience letters* Vol.397 (3) (Apr. 2006), p.240–244.
[41] J. Dennis et al. "Lower extremity joint angle, moment, and coordination throughout a double limb drop vertical jump in individuals with anterior cruciate ligament reconstruction". In: *Sports biomechanics* (May 2024), p.1–16.
[42] E. Mercado-Palomino et al. "Can kinematic and kinetic differences between planned and unplanned volleyball block jump-landings be associated with injury risk factors?" In: *Gait posture* Vol.79 (June 2020), p.71–79.
[43] M. Decker et al. "Gender differences in lower extremity kinematics, kinetics and energy absorption during landing". In: *Clinical biomechanics (Bristol)* Vol.18 (7) (Aug. 2003), p.662–669.
[44] E. Kristianslund et al. "Sidestep cutting technique and knee abduction loading: implications for ACL prevention exercises". In: *British journal of sports medicine* Vol.48 (9) (May 2014), p.779–783.

[45] S.K. Hunter et al. "The Biological Basis of Sex Differences in Athletic Performance: Consensus Statement for the American College of Sports Medicine". In: *Medicine Science in Sports Exercise* Vol. 55(12) (Sept. 2023), p. 2328–2360.

[46] K.R. Ford et al. "Longitudinal Effects of Maturation on Lower Extremity Joint Stiffness in Adolescent Athletes". In: *The American journal of sports medicine* Vol.38 (9) (Sept. 2010), p.1829–1837.

Appendix

Use of Artificial Intelligence

In the interest of transparency and academic integrity, this section outlines the use of artificial intelligence tools during the preparation of this thesis. I made selective use of ChatGPT and Perplexity, solely as tools for linguistic and technical support. All content presented in this thesis, namely the ideas, analyses, and interpretations, originates from my own work, informed by relevant scientific literature and discussions with my supervisor. At no point were these AI tools used to generate original content or perform the scientific reasoning behind this work.

Their use was strictly limited to assisting with the rephrasing of text I had already written, improving the clarity and academic tone of certain sections. Moreover, any output generated, whether for rewording, academic enhancement or translation, was never accepted uncritically. All suggestions were carefully reviewed and systematically revised to ensure that they accurately reflected my intended meaning and met the standards of academic writing.

Additionally, I used ChatGPT to support the generation and refinement of code, particularly for producing and adapting graphical outputs. This included tasks such as automating repetitive modifications (renaming variables or adjusting figure labels) and improving the visual quality of plots. These uses were aimed at enhancing the presentation and efficiency of data visualization, without contributing to the conceptual or analytical content of the thesis. Accordingly, all scientific contributions remain entirely my own.

Python codes

PCA computation code

```
1
2
3  import pandas as pd
4  import numpy as np
5  import matplotlib.pyplot as plt
6  from sklearn.decomposition import PCA
7  from sklearn.preprocessing import StandardScaler
8  import glob
9  import seaborn as sns
10 import os
11 from factor_analyzer.rotator import Rotator
12
13
14 output_dir = '/Users/cha/UNIF/MASTER 2/TFE/Data/Results PCA'
15
16
17 def process_files(file_path, first_column_name="TIME"):
18
19     # First lign for column names
20     col_names = pd.read_csv(file_path, sep="\t", skiprows=1, nrows=1,
       header=None).iloc[0].astype(str)
21
22     # 5th lign for direction (X-Y-Z)
23     directions = pd.read_csv(file_path, sep="\t", skiprows=4, nrows=1,
       header=None).iloc[0].astype(str)
24
25
26     # Merge 2 ligns to have unique column names
27     new_col_names = col_names + "_" + directions
28
29     # New column names
30     df = pd.read_csv(file_path, sep="\t", skiprows=5, names=new_col_names)
31
32     # Rename Time for 1st column
33     df.columns.values[0] = first_column_name
34
35     # Normalize time column (0-100%)
36     df[first_column_name] = (df[first_column_name] - df[first_column_name
       ].min() ) / (df[first_column_name].max() - df[first_column_name].min())
       * 100
37
38     # Choose appropriate columns
39     df = df[['TIME', 'RKNEE_ANGLE_X', 'RANKLE_ANGLE_X','LKNEE_ANGLE_X', '
       LANKLE_ANGLE_X','RHIP_ANGLE_X', 'RHIP_ANGLE_Y', 'RHIP_ANGLE_Z', '
       LHIP_ANGLE_X', 'LHIP_ANGLE_Y', 'LHIP_ANGLE_Z', 'TRUNK_ROTATION_X', '
       TRUNK_ROTATION_Y', 'TRUNK_ROTATION_Z']]
40
41     # To adjust inversion in software
```

```
    df['LANKLE_ANGLE_X'] *= -1

    return df


planned_files = glob.glob('/Users/cha/UNIF/MASTER 2/TFE/Data/Planned/*.txt')
unplanned_files = glob.glob('/Users/cha/UNIF/MASTER 2/TFE/Data/Unplanned/*.txt')

male_files = glob.glob('/Users/cha/UNIF/MASTER 2/TFE/Data/Male/*.txt')
female_files = glob.glob('/Users/cha/UNIF/MASTER 2/TFE/Data/Female/*.txt')


def mean_files(file_list):

    # Apply process_files to each file
    all_dfs = [process_files(f) for f in file_list]

    # Check compatibility of files
    if not all(df.shape == all_dfs[0].shape for df in all_dfs):
        raise ValueError("All files must have the same number of rows and columns")

    # Compute mean matrix
    average_df = pd.concat(all_dfs).groupby(level=0).mean()

    return average_df


mean_planned = mean_files(planned_files)
mean_unplanned = mean_files(unplanned_files)

mean_male = mean_files(male_files)
mean_female = mean_files(female_files)


def save_figure(figure, filename):
    # To save figures in a specific folder on computer
    figure.savefig(os.path.join(output_dir, filename))
    plt.close(figure)


def perform_pca(data, n_components=None, label=""):

    data = data.drop(columns=['TIME'])

    # Standardization of data mean = 0 and variance = 1
    scaler = StandardScaler()
    X_scaled = scaler.fit_transform(data)

    # Perform PCA
```

```
    pca = PCA(n_components=n_components)
    X_pca = pca.fit_transform(X_scaled)

    # Create loading matrix (i.e., coefficients of each feature in each PC)
    loadings = pd.DataFrame(pca.components_.T, columns=[f'PC{i+1}' for i in range(pca.n_components_)], index=data.columns)

    # Apply Varimax rotation
    rotator = Rotator(method='varimax')
    rotated_components = rotator.fit_transform(pca.components_.T).T  # Attention    la transposition

    # New loading matrix rotated
    rotated_loadings = pd.DataFrame(rotated_components.T, columns=[f'PC{i+1}' for i in range(pca.n_components_)], index=data.columns)


    # Explained variance for each component
    explained_variance = pca.explained_variance_ratio_


    # Diagram explained variance for each component
    fig2 = plt.figure(figsize=(8, 5), dpi=300)
    x_values = range(1, len(explained_variance) + 1)
    plt.bar(x_values, explained_variance * 100, alpha=0.7, color='royalblue', label='Explained variance')
    plt.plot(x_values, explained_variance * 100, marker='o', color='blue', linestyle='-', label='Percentage of each PC')

    #Add %
    for i, v in enumerate(explained_variance * 100):
        plt.text(x_values[i], v + 1, f'{v:.2f}%', ha='center', fontsize=13, color='black')

    plt.xlabel('Principal Components', fontsize=15)
    plt.ylabel('Explained variance (%)', fontsize=15)
    plt.title(f'{label}', fontsize=14)
    plt.xticks(x_values)
    plt.legend(fontsize=14)
    plt.grid(axis='y')
    save_figure(fig2, f'explained_variance_{label}.png')
    plt.show()

    # Limit heatmap to 2 first components
    n_heatmap_components = 2
    loadings_subset = loadings.iloc[:, :n_heatmap_components]
    rotated_loadings_subset = rotated_loadings.iloc[:, :n_heatmap_components]

    # Heatmap des loadings Varimax rotated
    fig4 = plt.figure(figsize=(10, 5), dpi=300)
```

```
    sns.heatmap(abs(rotated_loadings_subset), annot=
    rotated_loadings_subset, cmap="RdPu", cbar_kws={'label': 'Weighted
    loading magnitude'})
    plt.title(f'{label} - Rotated Loadings', fontsize=14)
    plt.tight_layout()
    save_figure(fig4, f'rotated_loadings_heatmap_{label}.png')
    plt.show()

    # Return le DataFrame for PC
    pca_df = pd.DataFrame(X_pca, columns=[f'PC{i+1}' for i in range(X_pca.
    shape[1])])

    return pca_df, explained_variance


pca_df_planned, explained_variance_planned = perform_pca(mean_planned,
    n_components=4, label = "Planned")

pca_df_unplanned, explained_variance_unplanned = perform_pca(
    mean_unplanned, n_components=4, label ="Unplanned")


pca_df_male, explained_variance_male = perform_pca(mean_male, n_components
    =4, label = "Male")

pca_df_female, explained_variance_female = perform_pca(mean_female,
    n_components=4, label = "Female")
```

SPM1D computation code

```


import pandas as pd
import numpy as np
import matplotlib.pyplot as plt
from sklearn.decomposition import PCA
from sklearn.preprocessing import StandardScaler
import glob
import seaborn as sns
import os
import re
import spm1d
from factor_analyzer.rotator import Rotator


output_dir = '/Users/cha/UNIF/MASTER 2/TFE/Data/Results PCA'


def process_files(file_path, first_column_name="TIME"):

    # First lign for column names
```

```
    col_names = pd.read_csv(file_path, sep="\t", skiprows=1, nrows=1, header=None).iloc[0].astype(str)

    # 5th lign for direction (X-Y-Z)
    directions = pd.read_csv(file_path, sep="\t", skiprows=4, nrows=1, header=None).iloc[0].astype(str)


    # Merge 2 ligns to have unique column names
    new_col_names = col_names + "_" + directions

    # New column names
    df = pd.read_csv(file_path, sep="\t", skiprows=5, names=new_col_names)

    # Rename Time for 1st column
    df.columns.values[0] = first_column_name

    # Normalize time column (0-100%)
    df[first_column_name] = (df[first_column_name] - df[first_column_name].min() ) / (df[first_column_name].max() - df[first_column_name].min()) * 100

    #Choose appropriate columns
    df = df[['TIME', 'FP1_X', 'FP1_Y', 'FP1_Z', 'FP2_X', 'FP2_Y', 'FP2_Z']]

    return df


planned_files = glob.glob('/Users/cha/UNIF/MASTER 2/TFE/Data/Planned/*.txt')
unplanned_files = glob.glob('/Users/cha/UNIF/MASTER 2/TFE/Data/Unplanned/*.txt')

male_files = glob.glob('/Users/cha/UNIF/MASTER 2/TFE/Data/Male/*.txt')
female_files = glob.glob('/Users/cha/UNIF/MASTER 2/TFE/Data/Female/*.txt')

def mean_files(file_list):

    # Apply process_files to each file
    all_dfs = [process_files(f) for f in file_list]

    # Check compatibility of files
    if not all(df.shape == all_dfs[0].shape for df in all_dfs):
        raise ValueError("All files must have the same number of rows and columns")

    # Compute mean matrix
    average_df = pd.concat(all_dfs).groupby(level=0).mean()

    return average_df

```

```
66
67 def std_files(file_list):
68     # Apply process_files to each file
69     all_dfs = [process_files(f) for f in file_list]
70
71     # Concatenate all DataFrames to form a single large DataFrame with
       multi-index (index 0 = row, index 1 = file)
72     concat_df = pd.concat(all_dfs, keys=range(len(all_dfs)))
73
74     # Compute standard deviation (level = 1 because file index
75     std_df = concat_df.groupby(level=1).std()
76
77     return std_df
78
79
80
81 mean_planned = mean_files(planned_files)
82 std_planned = std_files(planned_files)
83
84 mean_unplanned = mean_files(unplanned_files)
85 std_unplanned = std_files(unplanned_files)
86
87 mean_male = mean_files(male_files)
88 std_male = std_files(male_files)
89
90 mean_female = mean_files(female_files)
91 std_female = std_files(female_files)
92
93
94
95 # Plot GRF Planned VS Unplanned
96 fig, axs = plt.subplots(1, 3, figsize=(14, 4), dpi=300)
97
98 colors = {'Right': 'forestgreen', 'Left': 'darkorange'}
99
100 y_labels = ['Mediolateral GRF (N)', 'Anteroposterior GRF (N)', 'Vertical
       GRF (N)']
101 components = ['X', 'Y', 'Z']
102
103 all_handles = []
104 all_labels = []
105
106 for i in range(3):
107     comp = components[i]
108
109     line1, = axs[i].plot(mean_planned['TIME'], mean_planned[f'FP1_{comp}'
       ], color=colors['Right'], linewidth=1.5, label="Right (Planned)")
110     line2, = axs[i].plot(mean_planned['TIME'], mean_planned[f'FP2_{comp}'
       ], color=colors['Left'], linewidth=1.5, label="Left (Planned)")
111
112     line3, = axs[i].plot(mean_unplanned['TIME'], mean_unplanned[f'FP1_{
       comp}'], color=colors['Right'], linewidth=1.5, linestyle='--', label="
```

```
    Right (Unplanned)")
113     line4, = axs[i].plot(mean_unplanned['TIME'], mean_unplanned[f'FP2_{
    comp}'], color=colors['Left'], linewidth=1.5, linestyle='--', label="
    Left (Unplanned)")
114
115     axs[i].set_xlabel('Time (%)', fontsize=15)
116     axs[i].set_ylabel(y_labels[i], fontsize=15)
117     axs[i].grid(True)
118
119     if i == 0:
120         all_handles = [line1, line2, line3, line4]
121         all_labels = [line.get_label() for line in all_handles]
122
123 # Shared legend
124 fig.legend(all_handles, all_labels, loc='lower center', ncol=4, frameon=
    False, bbox_to_anchor=(0.5, -0.05), fontsize=14)
125 # Adjustment
126 fig.tight_layout(rect=[0, 0.08, 1, 1])
127
128 fig.savefig(os.path.join(output_dir, 'GRF_combined.png'), bbox_inches='
    tight')
129 plt.show()
130
131
132 ### Preparation for spm1d computation ###
133
134 def process_files_resampled(file_path, first_column_name="TIME", n_points
    =101):
135     # Lecture et pr paration des colonnes
136     col_names = pd.read_csv(file_path, sep="\t", skiprows=1, nrows=1,
    header=None).iloc[0].astype(str)
137     directions = pd.read_csv(file_path, sep="\t", skiprows=4, nrows=1,
    header=None).iloc[0].astype(str)
138     new_col_names = col_names + "_" + directions
139     df = pd.read_csv(file_path, sep="\t", skiprows=5, names=new_col_names)
140     df.columns.values[0] = first_column_name
141
142     # Time normalization
143     df[first_column_name] = (df[first_column_name] - df[first_column_name
    ].min()) / (df[first_column_name].max() - df[first_column_name].min())
    * 100
144
145     df = df[['TIME', 'FP1_X', 'FP1_Y', 'FP1_Z', 'FP2_X', 'FP2_Y', 'FP2_Z'
    ]]
146
147
148     new_time = np.linspace(0, 100, n_points)
149     new_data = {'TIME': new_time}
150
151     # Interpolation for each column except TIME
152     for col in df.columns:
153         if col != 'TIME':
```

```
            new_data[col] = np.interp(new_time, df['TIME'], df[col])

    df_resampled = pd.DataFrame(new_data)

    return df_resampled


def extract_all_components(file_list):

    components = ['FP1_X', 'FP1_Y', 'FP1_Z', 'FP2_X', 'FP2_Y', 'FP2_Z']
    data = {comp: [] for comp in components}

    for f in file_list:
        df = process_files_resampled(f)
        for comp in components:
            data[comp].append(df[comp].values)

    # Convert en np.array (n_trials x n_timepoints)
    for comp in components:
        data[comp] = np.array(data[comp])

    return data


planned_data = extract_all_components(planned_files)
unplanned_data = extract_all_components(unplanned_files)


planned_spm1d = {}
for comp in ['FP1_X', 'FP1_Y', 'FP1_Z', 'FP2_X', 'FP2_Y', 'FP2_Z']:
    planned_spm1d[f"{comp}"] = planned_data[comp]

unplanned_spm1d = {}
for comp in ['FP1_X', 'FP1_Y', 'FP1_Z', 'FP2_X', 'FP2_Y', 'FP2_Z']:
    unplanned_spm1d[f"{comp}"] = unplanned_data[comp]



### spm1d plots ###

# Planned VS Unplanned Left


fig, axs = plt.subplots(2, 3, figsize=(18, 10), dpi=300, gridspec_kw={'
    height_ratios': [1, 1]})

labels = ['FP2_X', 'FP2_Y', 'FP2_Z']
titles = ['Mediolateral GRF (N)', 'Anteroposterior GRF (N)', 'Vertical GRF
    (N)']
time = np.linspace(0, 100, planned_spm1d[labels[0]].shape[1])  # en
    supposant temps normalis     100%

```

```
for i, label in enumerate(labels):
    # Mean    SD
    ax_top = axs[0, i]
    mean_planned = np.mean(planned_spm1d[label], axis=0)
    std_planned = np.std(planned_spm1d[label], axis=0)
    mean_unplanned = np.mean(unplanned_spm1d[label], axis=0)
    std_unplanned = np.std(unplanned_spm1d[label], axis=0)

    ax_top.plot(time, mean_planned, color='darkorange', label='Planned')
    ax_top.fill_between(time, mean_planned - std_planned, mean_planned +
   std_planned, color='darkorange', alpha=0.25)

    ax_top.plot(time, mean_unplanned, color='darkorange',linestyle = '--',
    label='Unplanned')
    ax_top.fill_between(time, mean_unplanned - std_unplanned,
   mean_unplanned + std_unplanned, color='darkorange', linestyle = '--',
   alpha=0.15)

    ax_top.axhline(y=0, color='k', linestyle=':')
    ax_top.set_xlim([0, 100])
    ax_top.margins(x=0)
    ax_top.set_title(titles[i], fontsize=18)
    ax_top.set_xlabel('Time (%)', fontsize=16)
    ax_top.set_ylabel('Force (N)', fontsize=16)
    ax_top.legend(fontsize=13)

    # SPM t test
    ax_bottom = axs[1, i]
    t = spm1d.stats.ttest_paired(planned_spm1d[label], unplanned_spm1d[
   label])
    ti = t.inference(alpha=0.05, two_tailed=True)
    ti.plot(ax=ax_bottom)
    ti.plot_threshold_label(ax=ax_bottom, fontsize=12)
    ti.plot_p_values(ax=ax_bottom, size=12)
    ax_bottom.set_xlabel('Time (%)', fontsize=16)
    ax_bottom.set_ylabel('SPM{t}', fontsize=16)

fig.suptitle('Planned vs. Unplanned - Left', fontsize=22)

plt.tight_layout(rect=[0, 0.03, 1, 0.95])
fig.savefig(os.path.join(output_dir, 'GRF_spm1d_with_meanSD_Left_PvsU.png'
   ), bbox_inches='tight')
plt.show()



# Planned VS Unplanned Right

fig, axs = plt.subplots(2, 3, figsize=(18, 10), dpi=300, gridspec_kw={'
   height_ratios': [1, 1]})

labels = ['FP1_X', 'FP1_Y', 'FP1_Z']
```

```
titles = ['Mediolateral GRF (N)', 'Anteroposterior GRF (N)', 'Vertical GRF (N)']
time = np.linspace(0, 100, planned_spm1d[labels[0]].shape[1])  # Suppos en % du temps

for i, label in enumerate(labels):
    # Mean    SD
    ax_top = axs[0, i]
    mean_planned = np.mean(planned_spm1d[label], axis=0)
    std_planned = np.std(planned_spm1d[label], axis=0)
    mean_unplanned = np.mean(unplanned_spm1d[label], axis=0)
    std_unplanned = np.std(unplanned_spm1d[label], axis=0)

    ax_top.plot(time, mean_planned, color='forestgreen', label='Planned')
    ax_top.fill_between(time, mean_planned - std_planned, mean_planned + std_planned, color='forestgreen', alpha=0.25)

    ax_top.plot(time, mean_unplanned, color='forestgreen', linestyle = '--', label='Unplanned')
    ax_top.fill_between(time, mean_unplanned - std_unplanned, mean_unplanned + std_unplanned, color='forestgreen', linestyle = '--', alpha=0.15)

    ax_top.axhline(y=0, color='k', linestyle=':')
    ax_top.set_xlim([0, 100])
    ax_top.margins(x=0)
    ax_top.set_title(titles[i], fontsize=18)
    ax_top.set_xlabel('Time (%)', fontsize=16)
    ax_top.set_ylabel('Force (N)', fontsize=16)
    ax_top.legend(fontsize=13)

    # SPM t-test
    ax_bottom = axs[1, i]
    t = spm1d.stats.ttest_paired(planned_spm1d[label], unplanned_spm1d[label])
    ti = t.inference(alpha=0.05, two_tailed=True)
    ti.plot(ax=ax_bottom)
    ti.plot_threshold_label(ax=ax_bottom, fontsize=12)
    ti.plot_p_values(ax=ax_bottom, size=12)
    ax_bottom.set_xlabel('Time (%)', fontsize=16)
    ax_bottom.set_ylabel('SPM{t}', fontsize=16)

fig.suptitle('Planned vs. Unplanned - Right', fontsize=22)

plt.tight_layout(rect=[0, 0.03, 1, 0.95])
fig.savefig(os.path.join(output_dir, 'GRF_spm1d_with_meanSD_Right_PvsU.png'), bbox_inches='tight')
plt.show()
```

```
# Left VS Right in Planned


fig, axs = plt.subplots(2, 3, figsize=(18, 10), dpi=300, gridspec_kw={'height_ratios': [1, 1]})

labels = ['FP1_X', 'FP1_Y', 'FP1_Z']
labels_left = ['FP2_X', 'FP2_Y', 'FP2_Z']
titles = ['Mediolateral GRF (N)', 'Anteroposterior GRF (N)', 'Vertical GRF (N)']
time = np.linspace(0, 100, planned_spm1d[labels[0]].shape[1])  # Time vector

for i in range(3):
    # Mean    SD
    ax_top = axs[0, i]
    mean_right = np.mean(planned_spm1d[labels[i]], axis=0)
    std_right = np.std(planned_spm1d[labels[i]], axis=0)
    mean_left = np.mean(planned_spm1d[labels_left[i]], axis=0)
    std_left = np.std(planned_spm1d[labels_left[i]], axis=0)


    ax_top.plot(time, mean_right, color='forestgreen', label='Right')
    ax_top.fill_between(time, mean_right - std_right, mean_right + std_right, color='forestgreen', alpha=0.2)


    ax_top.plot(time, mean_left, color='darkorange', label='Left')
    ax_top.fill_between(time, mean_left - std_left, mean_left + std_left, color='darkorange', alpha=0.2)

    ax_top.axhline(y=0, color='k', linestyle=':')
    ax_top.set_xlim([0, 100])
    ax_top.margins(x=0)
    ax_top.set_title(titles[i], fontsize=18)
    ax_top.set_xlabel('Time (%)', fontsize=16)
    ax_top.set_ylabel('Force (N)', fontsize=16)
    ax_top.legend(fontsize=13)

    # SPM t-test
    ax_bottom = axs[1, i]
    t = spm1d.stats.ttest_paired(planned_spm1d[labels[i]], planned_spm1d[labels_left[i]])
    ti = t.inference(alpha=0.05, two_tailed=True)
    ti.plot(ax=ax_bottom)
    ti.plot_threshold_label(ax=ax_bottom, fontsize=12)
    ti.plot_p_values(ax=ax_bottom, size=12)
    ax_bottom.set_xlabel('Time (%)', fontsize=16)
    ax_bottom.set_ylabel('SPM{t}', fontsize=16)


fig.suptitle('Left vs. Right - Planned', fontsize=22)
```

```
338
339 plt.tight_layout(rect=[0, 0.03, 1, 0.95])
340 fig.savefig(os.path.join(output_dir, 'GRF_spm1d_with_meanSD_planned_LvsR.
    png'), bbox_inches='tight')
341 plt.show()
342
343
344
345 # Left VS Right in Unplanned
346
347
348 fig, axs = plt.subplots(2, 3, figsize=(18, 10), dpi=300, gridspec_kw={'
    height_ratios': [1, 1]})
349
350 labels_right = ['FP1_X', 'FP1_Y', 'FP1_Z']
351 labels_left  = ['FP2_X', 'FP2_Y', 'FP2_Z']
352 titles = ['Mediolateral GRF (N)', 'Anteroposterior GRF (N)', 'Vertical GRF
     (N)']
353 time = np.linspace(0, 100, unplanned_spm1d[labels_right[0]].shape[1])  #
    vecteur temps en %
354
355 for i in range(3):
356     #  Mean    SD
357     ax_top = axs[0, i]
358     mean_right = np.mean(unplanned_spm1d[labels_right[i]], axis=0)
359     std_right = np.std(unplanned_spm1d[labels_right[i]], axis=0)
360     mean_left = np.mean(unplanned_spm1d[labels_left[i]], axis=0)
361     std_left = np.std(unplanned_spm1d[labels_left[i]], axis=0)
362
363
364     ax_top.plot(time, mean_right, color='forestgreen', linestyle='--',
    label='Right')
365     ax_top.fill_between(time, mean_right - std_right, mean_right +
    std_right, color='forestgreen', linestyle='--', alpha=0.2)
366
367     ax_top.plot(time, mean_left, color='darkorange', linestyle='--', label
    ='Left')
368     ax_top.fill_between(time, mean_left - std_left, mean_left + std_left,
    color='darkorange', linestyle='--', alpha=0.2)
369
370     ax_top.axhline(y=0, color='k', linestyle=':')
371     ax_top.set_xlim([0, 100])
372     ax_top.margins(x=0)
373     ax_top.set_title(titles[i], fontsize=18)
374     ax_top.set_xlabel('Time (%)', fontsize=16)
375     ax_top.set_ylabel('Force (N)', fontsize=16)
376     ax_top.legend(fontsize=13)
377
378     # SPM t-test
379     ax_bottom = axs[1, i]
380     t = spm1d.stats.ttest_paired(unplanned_spm1d[labels_right[i]],
    unplanned_spm1d[labels_left[i]])
```

```
    ti = t.inference(alpha=0.05, two_tailed=True)
    ti.plot(ax=ax_bottom)
    ti.plot_threshold_label(ax=ax_bottom, fontsize=12)
    ti.plot_p_values(ax=ax_bottom, size=12)
    ax_bottom.set_xlabel('Time (%)', fontsize=16)
    ax_bottom.set_ylabel('SPM{t}', fontsize=16)

fig.suptitle('Left vs. Right - Unplanned', fontsize=22)
plt.tight_layout(rect=[0, 0.03, 1, 0.95])
fig.savefig(os.path.join(output_dir, 'GRF_spm1d_with_meanSD_unplanned_LvsR
    .png'), bbox_inches='tight')
plt.show()
```